catalysts

MDPI

Article

Catalytic Oxidation of Dimethyl Disulfide over Bimetallic Cu–Au and Pt–Au Catalysts Supported on γ-Al_2O_3, CeO_2, and CeO_2–Al_2O_3

Tuomas K. Nevanperä [1], Satu Ojala [1,*], Tiina Laitinen [1], Satu Pitkäaho [1], Sami Saukko [2] and Riitta L. Keiski [1]

[1] Faculty of Technology, Environmental and Chemical Engineering, University of Oulu, P.O. Box 4300, FI-90014 Oulu, Finland

[2] Center of Microscopy and Nanotechnology, University of Oulu, P.O. Box 7150, FI-90014 Oulu, Finland

* Correspondence: satu.ojala@oulu.fi; Tel.: +358-50-350-6098

Received: 19 June 2019; Accepted: 12 July 2019; Published: 13 July 2019

Abstract: Dimethyl disulfide (DMDS, CH_3SSCH_3) is an odorous and harmful air pollutant (volatile organic compound (VOC)) causing nuisance in urban areas. The abatement of DMDS emissions from industrial sources can be realized through catalytic oxidation. However, the development of active and selective catalysts having good resistance toward sulfur poisoning is required. This paper describes an investigation related to improving the performance of Pt and Cu catalysts through the addition of Au to monometallic "parent" catalysts via surface redox reactions. The catalysts were characterized using ICP-OES, N_2 physisorption, XRD, XPS, HR-TEM, H_2-TPR, NH_3-TPD, CO_2-TPD, and temperature-programmed $^{18}O_2$ isotopic exchange. The performance of the catalysts was evaluated in DMDS total oxidation. In addition, the stability of a Pt–Au/Ce–Al catalyst was investigated through 40 h time onstream. Cu–Au catalysts were observed to be more active than corresponding Pt–Au catalysts based on DMDS light-off experiments. However, the reaction led to a higher amount of oxygen-containing byproduct formation, and thus the Pt–Au catalysts were more selective. H_2-TPR showed that the higher redox capacity of the Cu-containing catalysts may have been the reason for better DMDS conversion and lower selectivity. The lower amount of reactive oxygen on the surface of Pt-containing catalysts was beneficial for total oxidation. The improved selectivity of ceria-containing catalysts after the Au addition may have resulted from the lowered amount of reactive oxygen as well. The Au addition improved the activity of Al_2O_3-supported Cu and Pt. The Au addition also had a positive effect on SO_2 production in a higher temperature region. A stability test of 40 h showed that the Pt–Au/Ce–Al catalyst, while otherwise promising, was not stable enough, and further development is still needed.

Keywords: catalytic total oxidation; emission treatment; poisoning; environmental catalysis; gold; platinum; copper

1. Introduction

Volatile organic compounds (VOCs) are major contributors of direct (toxicity, ground level photochemical ozone formation) and indirect (smog formation, stratospheric ozone depletion, particulate matter formation) air pollution [1]. VOCs are also greenhouse gases (GHGs) with a GHG effect more than 50 times greater than the effect of CO_2. Sulfur-containing VOCs (SVOCs) originate from the wood industry, such as from pulping processes and chemical production as well as from landfill sites and wastewater treatment plants. Typical examples of SVOCs are methyl mercaptan (CH_3SH), dimethyl sulfide (CH_3SCH_3), and dimethyl disulfide (CH_3SSCH_3) [2], which are disturbingly malodorous, even at very low concentrations, and thus cause discomfort in urban areas. [3,4].

Catalytic treatment is a suitable abatement technology for VOCs, especially when emission streams are complex and when the total VOC concentrations fluctuate. Catalytic oxidation is an environmentally sound destructive method and is highly feasible economically when heat-recovery-allowing processes such as reverse flow reactors (RFRs) are used. Catalytic oxidation of SVOCs is an attractive possibility: However, due to the presence of sulfur, the selectivity and stability of the catalysts need to be improved [2].

The use of bimetallic catalysts in the total oxidation of gaseous dimethyl disulfide (DMDS) has not yet been extensively studied. Ojala [5] used Pt–Pd, Mn–Mg, Cu–Cr, and Cu–Mg–Cr catalysts supported on alumina or ceria–alumina in CH_3SH and CH_3SSCH_3 oxidation. Kucherov et al. [6,7] studied the removal of CH_3OH, CH_3SH, and CH_3SSCH_3 from flue gases using Au–Rh/HZSM-5 catalysts. The experiments demonstrated high activity and good sulfur resistance at temperatures as low as 290 °C. Darif et al. [8–10] studied the catalytic oxidation of CH_3SSCH_3 over Pt–Cu catalysts and reported similarly promising results.

Sulfate promotes the mobility of Pt particles on the catalyst support, which can lead to Pt agglomeration. Simultaneously, it hinders the redispersion of Pt during regeneration. According to Corro et al. [11], the high oxidation states of Pt are more sensitive to sulfur than lower oxidation states. In the work of Darif et al. [10], the 0.3Pt10Cu/Al_2O_3 catalyst having Pt(IV) species on its surface contained a higher amount of sulfur than the used 0.3Pt10Cu/Al_2O_3(20%)SiO_2 catalyst with Pt(II) on its surface. The Al_2O_3(20%)SiO_2 support played a protective role against sulfur poisoning, which was most likely due to its high acidity.

Our previous study focused on the use of supported monometallic catalysts in the total oxidation of dimethyl disulfide (CH_3SSCH_3). Cu and Pt catalysts were considered as reference materials, while monometallic Au was of a special interest due to its hypothesized sulfur resistance. Cu catalysts exhibited high activity in the oxidation of DMDS, but resulted in undesired final products and deactivation. In that study, the best catalyst was the Cu/Al catalyst, which should be operated above 600 °C to avoid the formation of formaldehyde (CH_2O) and carbon monoxide (CO). The problem was that at higher temperatures, the production of sulfur dioxide (SO_2), the desired reaction product, was decreased as well. Pt catalysts showed decent activity, but suffered similarly from a decline in the formation of SO_2 that might have been an indication of the production of unwanted SO_3. Au- and ceria-containing catalysts maintained the formation of SO_2 at high temperatures, but oxidation was not complete. Generally, Au seemed to promote a reaction toward total oxidation at high temperatures. The ceria–alumina-supported Au catalyst showed durability against sulfur poisoning, but the production of unwanted CH_2O was significant, and therefore the selectivity of the catalyst needed an improvement [12]. In this study, bimetallic catalysts were prepared to overcome the described problems. Au-promoted Pt and Cu catalysts supported on alumina, ceria, and ceria–alumina were prepared: We aimed for high activity, good selectivity toward both SO_2 and CO_2, as well as improved resistance against sulfur poisoning during the catalytic oxidation of DMDS.

2. Results

2.1. Characterization

The specific surface area (S_{BET}) values of the bimetallic catalysts are presented in Table 1. In comparison with the S_{BET} of "parent" monometallic catalysts, the S_{BET} values decreased after the addition of Au and the final calcination step. The decrease in the S_{BET} in the case of Al_2O_3-supported bimetallic catalysts was small, about 10 m^2 g^{-1}. However, in the case of CeO_2-supported "parent" catalysts, the decrease was drastic: From 190 to 65 m^2 g^{-1} and from 210 to 50 m^2 g^{-1}. In the case of CeO_2–Al_2O_3-supported bimetallic catalysts, S_{BET} values remained at a level similar to monometallic catalysts. N_2 sorption isotherms of all the prepared bimetallic catalysts (Supplementary Materials, Figure S1) corresponded to an IUPAC classification Type IV, which is typical for mesoporous materials. The shapes of the hysteresis loops were of Type H1, which is related to a well-defined cylindrical-like

pore structure or agglomerates of roughly uniform spheres [13]. The pore size distribution (Figure S2) in alumina and ceria–alumina samples were similar within a size range from a few nanometers to 200 nm. The ceria-supported catalyst had a higher number of micropores (from 5 to 40 nm) than the other catalysts. Parts of the pores of the ceria support were blocked during the Au addition to the "parent" catalyst, which was evidenced by a drastic decrease in the specific surface area.

According to the ICP-OES results displayed in Table 1, the targeted metal loadings of Pt and Cu were achieved rather well. The deposition of Au, however, was not successful in all the cases. As the target was 1 wt %, the catalysts showed an Au content of approximately 0.6–0.9 wt %, except for the Cu–Au/Ce catalyst, which had an Au loading of only 0.2 wt %. This might have been due to many reasons, such as different oxidation states and reduction potentials, support properties, or the deposition being restricted to the surface layers of parent metal and an excess of the Au modifier. In addition, the preparation conditions, reaction time, and dissociation of hydrogen on copper had an impact on the deposition of Au. The measured ceria content of CeO_2–Al_2O_3 was 20 wt %.

Table 1. Measured properties of the studied catalysts.

Catalyst	Support	S_{BET} [(a)] ($m^2\ g^{-1}$)	Total Pore Volume [(b)] ($cm^3\ g^{-1}$)	Average Pore Diameter [(b)] (nm)	Metal Loading (wt %)			Measured H_2 Consumption ($\mu mol\ g^{-1}$)
					Au	Pt	Cu	
Pt–Au/Al	Al_2O_3	95	0.49	19	0.8	0.9	-	44
Cu–Au/Al	Al_2O_3	90	0.48	19	0.6	-	4.7	1222
Pt–Au/Ce	CeO_2	65	0.17	9	0.6	1.1	-	781
Cu–Au/Ce	CeO_2	50	0.17	12	0.2	-	5.6	2566
Pt–Au/Ce–Al	CeO_2-Al_2O_3	85	0.41	18	0.9	1.1	-	315
Cu–Au/Ce–Al	CeO_2-Al_2O_3	75	0.37	18	0.6	-	5.9	1307

(a) Round values (±5); (b) cumulative pore volume between diameters of 1.7 nm and 300 nm; S_{BET}: Specific surface area.

The XRD diffraction patterns of the catalysts are shown in Figure 1. The phases observed matched with the peak positions of Al_2O_3 (gamma, JCPDS 056-1186), CeO_2 (cerianite, JCPDS 043-1002), Au (metallic, JCPDS 071-3755), and CuO (JCPDS 089-5895). In the case of alumina-supported catalysts (Figure 1a), it was difficult to distinguish between Pt, Au, Cu, and Al, since the corresponding peaks of the support and the dispersed metal were very close to each other.

In the case of ceria-supported catalysts (Figure 1b), despite very low loading, metallic Au could be clearly observed from the XRD diffractograms. This was most probably due to the large particle size of Au caused by sintering during the final calcination, which was facilitated by the presence of residual Cl on the catalyst surface from the used precursor and hydrochloric acid. Compared to the parent catalysts (Pt/Ce and Cu/Ce), the cerianite peaks were significantly more intense in the case of bimetallic catalysts, suggesting a more crystalline phase of cerianite. In addition, the specific surface area was significantly lower for the bimetallic catalyst. This proved that the ceria support of the parent catalyst was modified during the addition of Au. The Au crystallite size calculated based on the Scherrer equation was 44 nm for Au–Pt/Ce and 59 nm for Cu–Au/Ce.

In the case of ceria–alumina-supported catalysts (Figure 1c), Cu and Pt species were not observed from the diffractograms. Au could be identified from both the catalysts: However, the separation of the corresponding peaks from that of the support were not as clear as in the case of CeO_2-supported catalysts, despite the higher loading of Au.

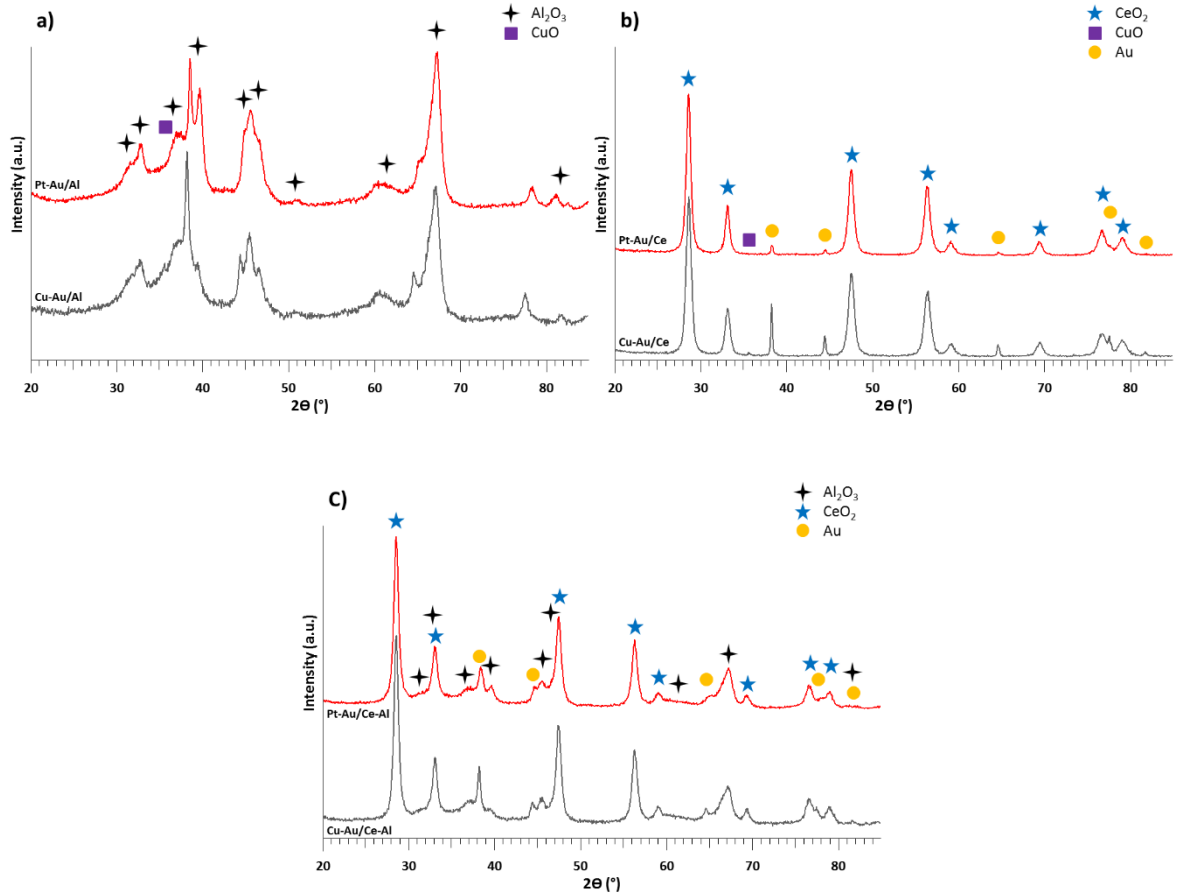

Figure 1. XRD diffractograms of (**a**) Pt–Au and Cu–Au on γ-Al_2O_3, (**b**) Pt–Au and Cu–Au on CeO_2, and (**c**) Pt–Au and Cu–Au on CeO_2–Al_2O_3 supports.

In our case, copper was not seen clearly in the XRD diffractograms, but very low-intensity peaks at 35.5° on alumina and ceria were roughly visible. The lack of high-intensity peaks was likely due to small two- and three-dimensional copper–oxygen clusters that could not be detected by XRD in contrast to large three-dimensional clusters and bulk CuO, which exhibited characteristics similar to the pure CuO powder visible in the XRD [14]. Pt was not detected due to its small loading and assumed small particle size.

Figure 2a–f show typical HR-TEM images of the prepared catalysts. The particle size distribution (PSD) in each catalyst was calculated based on Feret's diameter due to the irregular shape of the particles. As seen in Figure 2a, the Pt–Au/Al catalyst contained quite evenly dispersed particles, mainly in sizes of roughly 10–30 nm. Multiple EDX spectra analyzed from the HR-TEM images of the Pt–Au/Al catalyst showed that spherical particles contained more Au than Pt, whereas irregular grains contained more Pt than Au (Supplementary Materials, Figure S3) (needle-looking forms in the HR-TEM images are side views of the Al_2O_3 2D plates). Figure 2b displays an image of the Cu–Au/Al catalyst, which showed fairly homogeneously dispersed particles mainly in a size range from 10 to 50 nm. Some of the images showed "islands" of aggregated particles in sizes of a few hundreds of nanometers as well as unevenly distributed smaller particles (Figure S4). The agglomerates were a result of sintering during calcination, which was possible since the calcination temperature used during the preparation of bimetallic catalysts (600 °C) was higher than the Tammann ($0.5T_{melting}$) and Hüttig ($0.3T_{melting}$) temperatures of Au, Cu, CuO, and Cu_2O and higher than the Hüttig temperature of Pt (Table 2). The EDX spectrum of the particle shown in Figure 2b evidenced the presence of Au (Figure S4, EDX spectrum 3). The presence of Cu could not be validated due to the Cu grid used in the sample preparation.

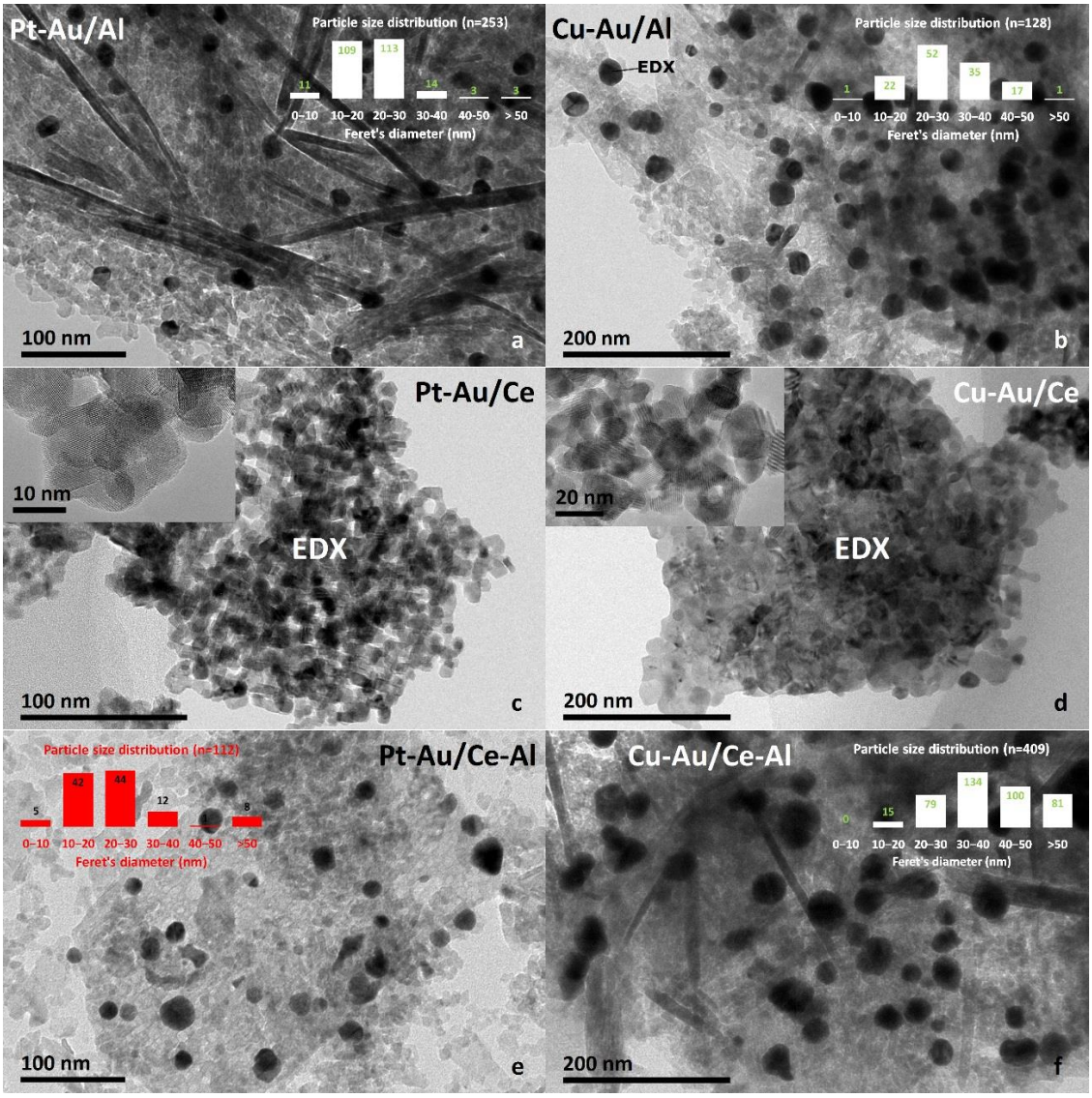

Figure 2. HR-TEM images of the prepared catalysts: (**a**) Pt–Au/Al, (**b**) Cu–Au/Al, (**c**) Pt–Au/Ce, (**d**) Cu–Au/Ce, (**e**) Pt–Au/Ce–Al, and (**f**) Cu–Au/Ce–Al.

Table 2. Melting point, Tammann, and Hüttig temperatures (converted from kelvin) for dispersed metals and their oxide forms (modified from Moulijn et al. [15]).

Compound	$T_{melting}$ (°C)	$T_{Tammann}$ (°C)	$T_{Hüttig}$ (°C)
Pt	1755	741	335
PtO	550	139	-26
PtO_2	450	89	-56
Au	1063	395	128
Cu	1083	405	134
CuO	1326	527	207
Cu_2O	1235	481	179

The HR-TEM images of Pt–Au/Ce and Cu–Au/Ce catalysts in Figure 2c,d show how difficult it was to distinguish the particles from each other. The EDX spectrum measured from the surface shown in Figure 2c confirmed the presence of Pt and Au. Some randomly dispersed Pt–Au agglomerates in sizes from 10 to 100 nm were found in the Pt–Au/Ce catalyst (Figure S5). The EDX spectrum taken from the surface of the Cu–Au/Ce catalyst shown (Figure 2d) verified the presence of Au (Figure S6).

The images of the Ce–Al-supported catalyst in Figure 2e,f show homogeneously dispersed particles. Some areas of the catalyst contained isolated islands of agglomerated Pt–Au particles (Figure S7). Similarly to the case of alumina-supported catalysts, EDX showed that spherical particles contained more Au than Pt, whereas irregularly shaped particles contained more Pt than Au (Figure S8). The particle size distribution of the Pt–Au/Ce–Al catalyst was from 10 to 40 nm. Spherical particles and islands of big agglomerates were observed. The particle size distribution of the Cu–Au/Ce–Al catalyst showed the presence of a higher number of larger particles (40–50 nm and >50 nm).

Figure 3a,b illustrates hydrogen consumptions during the H_2-TPR experiment for the calcined Pt–Au and Cu–Au catalysts. The measured H_2 consumptions are shown in Table 1. The effect of support was removed from the H_2 uptakes. In our previous work with the same supports, the γ-Al_2O_3 support did not show consumption of H_2 between 35 °C and 400 °C, as expected. Bare CeO_2 and CeO_2–Al_2O_3 supports showed typical H_2 consumptions starting roughly at 350 °C due to the presence of ceria [12].

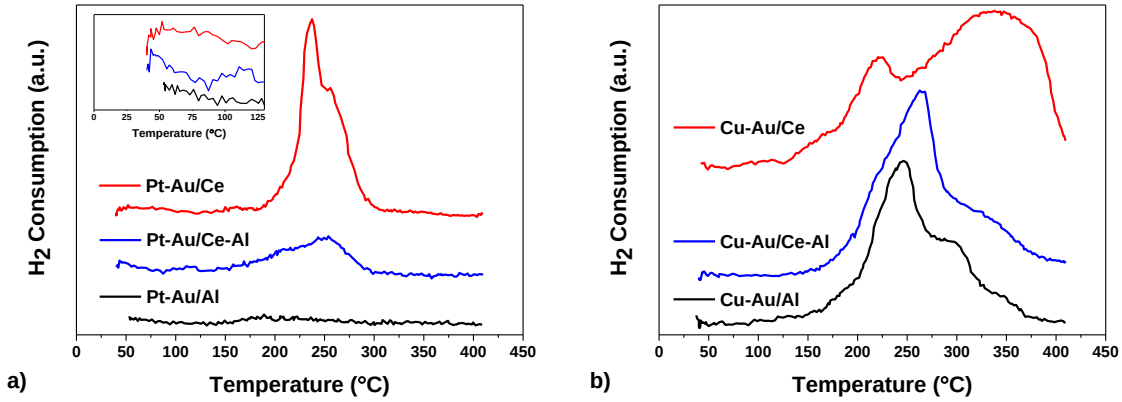

Figure 3. H_2-TPR profiles of (**a**) Pt–Au and (**b**) Cu–Au on γ-Al_2O_3, CeO_2, and CeO_2–Al_2O_3 supports. Total H_2 consumptions: Pt–Au/Al, 44 μmol g^{-1}; Pt–Au/Ce–Al, 315 μmol g^{-1}; Pt–Au/Ce, 781 μmol g^{-1}; Cu–Au/Al, 1222 μmol g^{-1}; Cu–Au/Ce–Al, 1307 μmol g^{-1}; Cu–Au/Ce, 2566 μmol g^{-1}.

Figure 3a shows the H_2-TPR profiles of the bimetallic catalysts prepared from Pt-containing "parent" catalysts. The TPR profile of the Pt–Au/Al catalyst was very similar to the Pt/Al "parent" catalyst, and no significant changes in the reduction behavior after the Au addition could be seen. A very low hydrogen uptake was seen at low temperatures of up to 80 °C that could have resulted in the reduction of Pt species or adsorbed oxygen species. Another slight uptake of H_2 for the Pt–Au/Al catalyst was detected between a broad temperature range of 150–300 °C. As the catalysts were calcined up to 600 °C, gold was probably reduced to Au^0 [16], and consequently the reduction of gold was not observed in either of the cases, i.e., monometallic Au/Al and bimetallic Pt–Au/Al. The addition of Au on the Pt/Ce–Al catalyst shifted the reduction of the catalyst by about 50 °C to higher temperatures. However, in the case of Pt/Ce, the effect of Au was opposite, and the uptake temperature of H_2 decreased significantly by about 160 °C. The location of this peak (at 240°C with a shoulder at 255 °C) was between the observed reduction of monometallic Au/Ce (at around 125 °C) and Pt/Ce (at around 400 °C).

The results of H_2-TPR for the bimetallic catalysts based on the Cu-containing "parent" catalysts are presented in Figure 3b. The addition of Au made the reduction of the Cu-containing "parent" catalysts more difficult by shifting the reduction temperature to a higher temperature region. In the case of Au–Cu/Ce, the shift was the most significant, over 100 °C. In all the cases, the H_2 consumption was lower than in the case of monometallic catalysts. The shapes of the peaks indicating H_2 consumption were also affected. The first peak in the case of Cu–Au/Al was almost two times higher than the second peak compared to the peaks seen with Cu/Al, which were almost equal. In the case of Cu–Au/Ce, the observation was opposite: The lower temperature peak was significantly smaller compared to the

higher temperature peak. These changes might have been due to differences in the particle size and/or interaction of copper species with the support oxide. Both of the reduction peaks were most probably related to Cu^{2+}, because transformation of Cu^{+} to Cu^{0} is typically observed at higher temperatures than those presented in Figure 3 [17]. A low temperature peak is typically assigned to small well-dispersed copper species that are weakly interacting with the support. Details of the reduction behavior of monometallic parent catalysts can be found in Reference [12].

In general, it seems that the addition of Au to the monometallic (Cu and Pt) catalysts made the reduction of the catalyst more difficult, except in the case of Pt/Ce. The reduction temperatures moved toward higher levels, and the total H_2 consumptions decreased. In the case of Pt/Ce, even the total hydrogen uptake was decreased after Au addition, and the reduction started at a significantly lower temperature. It is known that H_2 can be dissociated only on very small (smaller than clusters of 20 atoms) Au particles [18,19], which could explain why the reduction was more difficult after the addition of Au in our case (we expect that Au was in close contact with Pt or Cu due to the preparation method used). The H_2-TPR experiments showed that the Cu–Au catalysts consumed more H_2 than the Pt–Au catalysts did, meaning that the Cu–Au catalysts contained more reactive oxygen than the Pt–Au catalysts. Therefore, copper oxides could provide a quantity of oxygen at a lower temperature directly from their structure (Mars van Krevelen reaction mechanism) higher than the Pt–Au catalysts could dissociate (Langmuir–Hinshelwood reaction mechanism) from the gas phase. This may have had an impact on the performance of the catalyst.

XPS measurements were used to identify the surface composition and surface metal loadings of the catalysts (Table 3). Pt, Au, and Cu contents close to the surface were higher than the bulk metal loadings determined by ICP-OES, except in the case of Cu–Au/Ce. This could be explained by very low loading of Au and the accuracy of the measurements.

Table 3. Surface compositions of the catalysts.

Catalyst	XPS					
	Surface Composition (wt %)					
	Au	**Pt**	**Cu**	**Ce**	**Al**	**O**
Pt–Au/Al	0.9	1.2	-	-	51.3	46.6
Cu–Au/Al	5.2	-	7.5	-	46.1	41.2
Pt–Au/Ce	0.9	3.6	-	66.6	-	29.0
Cu–Au/Ce	0.1	-	12.4	61.1	-	26.4
Pt–Au/Ce–Al	2.2	2.1	-	4.4	48.1	43.2
Cu–Au/Ce–Al	4.0	-	8.6	2.2	45.4	39.9

The binding energy of the Au 4f spectra is shown in Figure 4. For all the catalysts, the main binding energy peaks of Au $4f_{7/2}$ and Au $4f_{5/2}$ between 83.1 and 83.8 eV and 86.8 and 87.5 eV, respectively, indicated metallic Au^{0}. Typically, the oxidation states of Au are determined from the Au $4f_{7/2}$ peak [20]. The observed binding energy values were slightly lower than those of the bulk metallic Au (Au $4f_{7/2}$ = 84.0 eV and Au $4f_{5/2}$ = 87.7 eV), but similar results for Au^{0} on the surfaces of catalysts have been previously reported in the literature [21–24]. Differences in the binding energy values could have been due to metal–support and/or metal–metal interactions [21,22,24]. Based on the preparation method of the bimetallic catalysts, we expected to have Au–Pt and Au–Cu interactions on the catalysts.

The Au 4f spectra for the Pt–Au/Ce catalyst also showed the oxidation state of Au^{1+} with a binding energy at 84.2 eV (indicated in Figure 4). The difference of about 0.6 eV between the binding energies of Au^{0} and Au^{1+} supports the presence of the oxidation state Au^{1+} [25]. Additionally, Au^{0} exhibited a theoretical intensity ratio of I(Au $4f_{7/2}$):I(Au $4f_{5/2}$) = 4:3 [26], which was used as one of the constraints in the fitting of the XPS data. However, the Au^{1+} peak might also have been caused by very small (<1.5 nm) Au particles on the surface [25,27,28]. High-angle annular dark-field scanning transmission electron microscope (HAADF-STEM) images demonstrated a possibility of the presence of very small

particles in addition to the larger particles observed with XRD (Supplementary Materials, Figure S9). In general, the Au $4f_{7/2}$ binding energy of ceria-supported bimetallic catalysts shifted toward lower binding energy values compared to the monometallic Au catalyst. The opposite behavior was observed for the alumina and ceria–alumina-supported bimetallic catalysts.

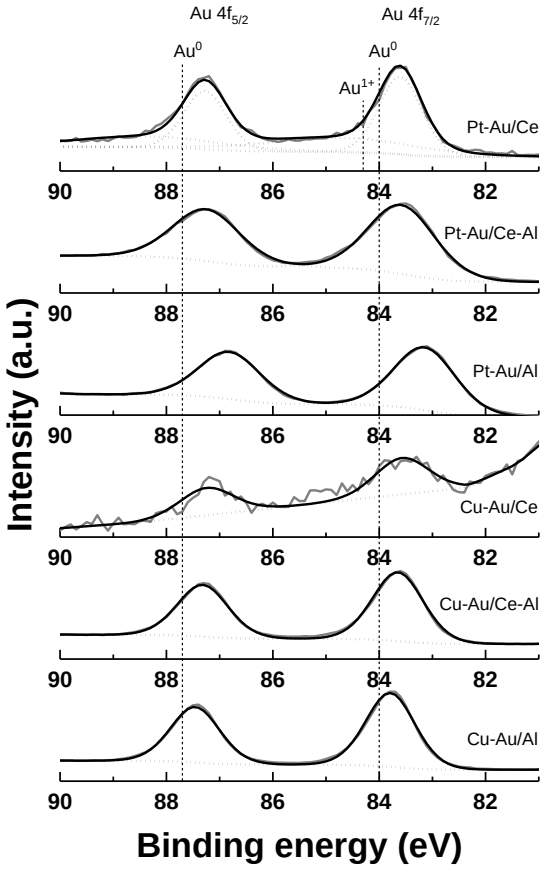

Figure 4. Au 4f spectra of all the studied catalysts (Au^0, indicated in the figure, is the theoretical binding energy value of Au^0).

Figure 5 presents the XPS spectra of Pt 4d and Pt 4f. Usually, most intense lines of platinum (Pt 4f lines) are used in the analysis of platinum species, but in the cases of the Pt–Au/Ce–Al and Pt–Au/Al catalysts, the Pt 4f line overlapped with the aluminum spectral line. For that reason, the Pt 4d line was used in the analysis.

The Pt 4f spectra for the Pt–Au/Ce catalyst showed two different oxidation states of platinum. According to the literature, the two peaks at 76.0 and 72.7 eV are assigned to Pt^{2+}, and the peaks at 77.2 and 74.4 eV are assigned to Pt^{4+} [8,29,30].

In the Pt–Au/Ce–Al and Pt–Au/Al catalysts, the binding energies at 313.2 eV and 313.0 eV, respectively, indicated a Pt^0 state. Typically, Pt^0 values are higher (at around 315 eV), but the reduction of catalysts at high temperatures decreases the Pt^0 binding energy values [31]. During the preparation, the catalysts were reduced in an H_2 flow at 300 °C for 1 h after the deposition of Au and were then calcined at 600 °C for 5 h. The peak shift might also have originated from metal–support and metal–metal interactions. Binding energies of 316.4 eV for Pt–Au/Al and Pt–Au/Ce–Al indicated the presence of a Pt^{2+} or Pt^{4+} state [8,31].

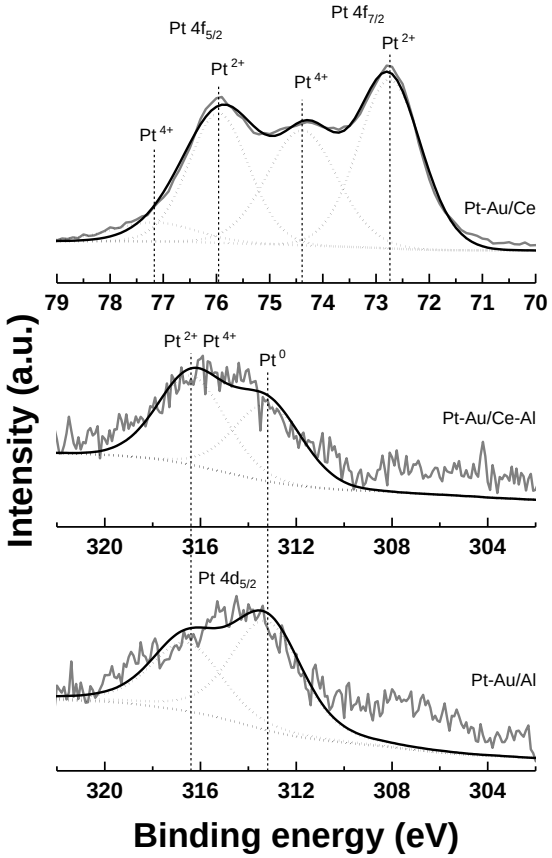

Figure 5. Pt 4f spectra of the Pt–Au/Ce catalyst and Pt 4d spectra of the Pt–Au/Ce–Al and Pt–Au/Al catalysts.

The Cu 2p spectra (shown in Figure 6) showed two spin-orbit multiples, which corresponded to Cu $2p_{3/2}$ (*BE* ~933 eV) and Cu $2p_{1/2}$ (*BE* ~953 eV) ionizations [20]. According to the literature, Cu 2p spectra contain shake-up peaks between 940 eV and 947 eV, and near 962.0 eV [32]. The Cu–Au/Ce catalyst did not show a shake-up peak near 962.0 eV, in contrast to Cu–Au/Ce–Al and Cu–Au/Al. This indicates that Cu–Au/Ce contained more Cu_2O (or Cu^0) than other catalysts [33] (the main peak for metallic Cu^0 and/or Cu_2O species is visible at a binding energy of 932.7 eV [20,34,35]). Because Cu–Au/Ce also showed shake-up peaks between 940 eV and 947 eV, the presence of CuO in the catalyst is possible. In the Cu–Au/Ce–Al and Cu–Au/Al catalysts, peaks observed at 933.1 eV and 933.7 eV, respectively, indicated the presence of CuO species [32,36]. This was supported by the appearance of shake-up peaks near 962.0 eV and between 940 eV and 947 eV. Binding energy values between 935.2 and 938.0 eV could refer to the interaction between copper and the support [36].

The XPS spectra of Ce 3d are shown in Figure 7. According to the literature, Ce 3d spectra show two spin-orbit multiples that correspond to Ce $3d_{3/2}$ (u) and Ce $3d_{5/2}$ (v) ionizations. The binding energy values of u', v' indicate the oxidation state of Ce^{3+}. Other observed peaks are related to Ce^{4+} [21,37,38].

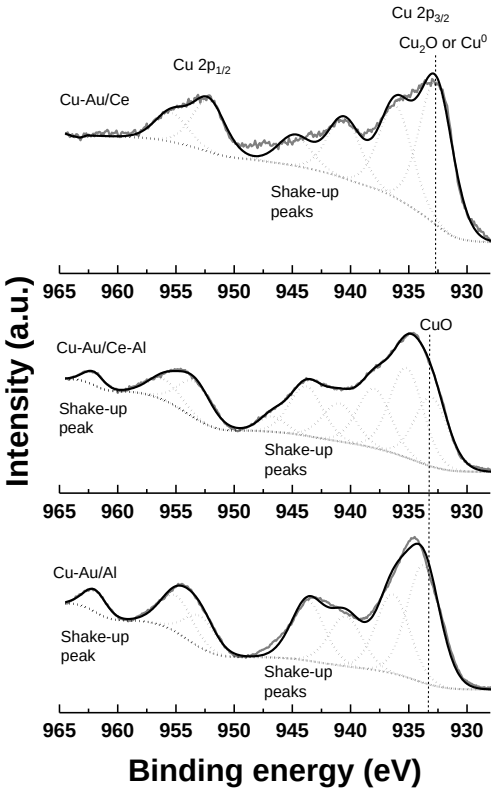

Figure 6. Cu 2p spectra of all Cu-containing catalysts.

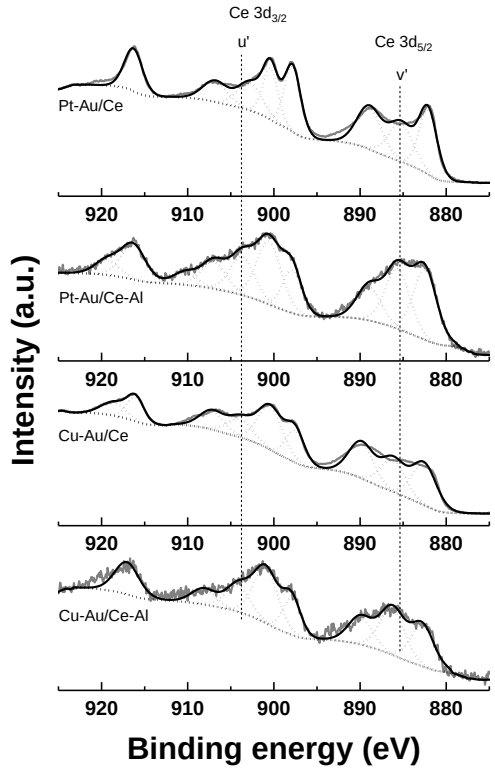

Figure 7. Ce 3d spectra of ceria-containing catalysts.

Based on the XPS results, ceria-supported bimetallic catalysts were slightly different from alumina and alumina–ceria-supported catalysts. Au was also observed at oxidation state +1 on ceria, while it was Au^0 on the other supports. The Pt–Au/Ce catalyst contained significantly more Pt^{2+} in addition to

Pt^{4+} than the other two catalysts, which also contained Pt^0. Thus, the amounts of higher oxidation states of Au and Pt were more pronounced on ceria. Copper XPS analysis showed opposite results, since the presence of lower oxidation states of Cu were observed on the ceria support. These results might have originated from the well-known redox behavior of ceria. The higher oxidation state of Au and Pt may be one explanation for the different behavior of the ceria-supported catalyst during H_2-TPR compared to other Pt–Au catalysts. Changes in the Au $4f_{7/2}$ binding energies between the monometallic and bimetallic catalysts indicated the presence of metal–metal interactions. This is supported by References [26,39].

Thermally programmed isotopic exchange (TPIE) experiments with labeled oxygen were conducted for all the catalysts. Graphs representing the rate of oxygen exchange (R_e) and the number of exchanged oxygen atoms (N_e) with respect to temperature are displayed in Figure 8a–f, respectively, and summarized in Table 4.

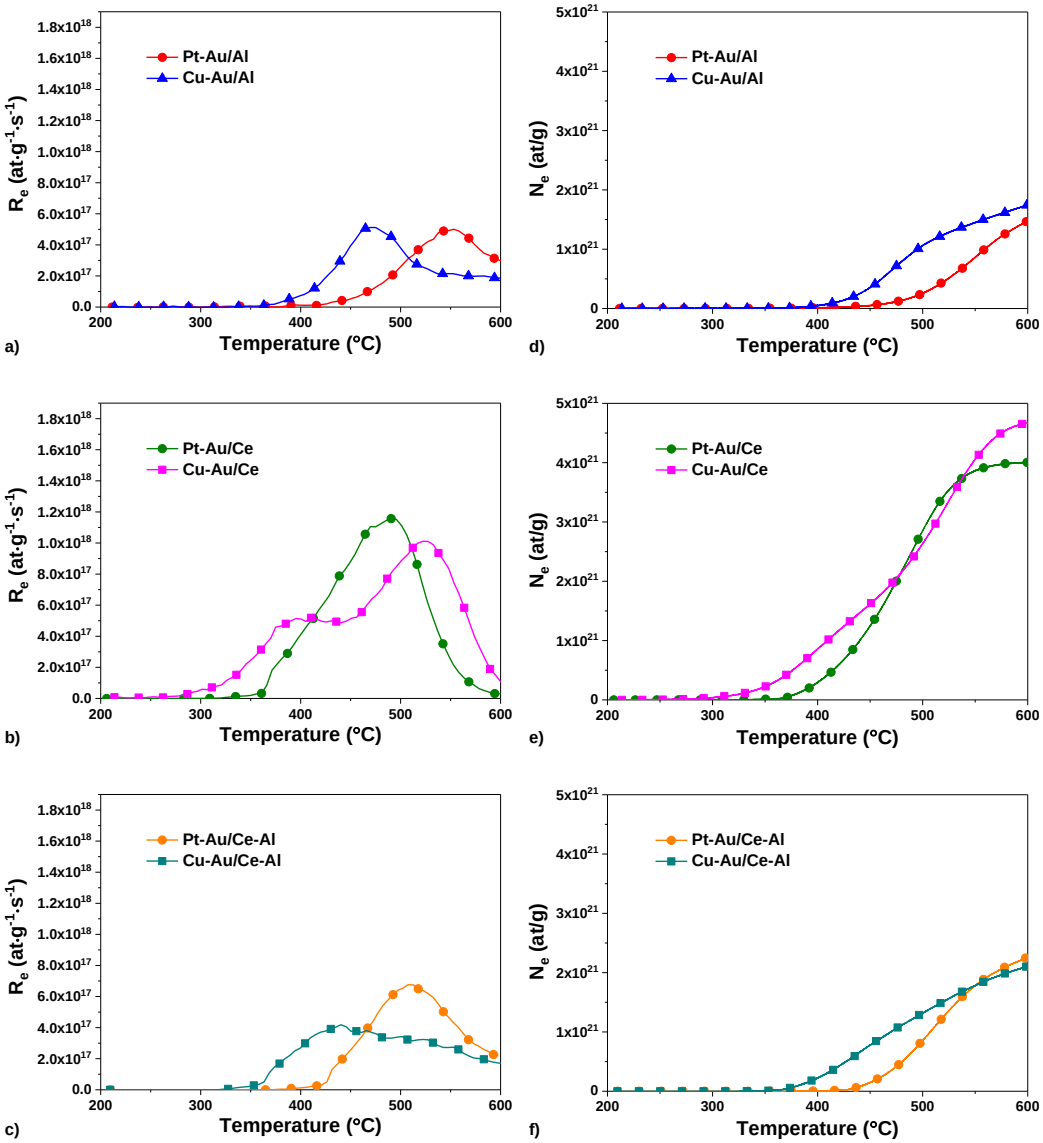

Figure 8. Evolution of the rate of oxygen exchange for Pt–Au and Cu–Au on (**a**) γ-Al_2O_3, (**b**) CeO_2, and (**c**) CeO_2–Al_2O_3 catalysts (R_e = rate of oxygen exchange) and evolution of the number of exchanged oxygen atoms for Pt–Au and Cu–Au on (**d**) γ-Al_2O_3, (**e**) CeO_2, and (**f**) CeO_2–Al_2O_3 catalysts (N_e = number of exchanged oxygen atoms) in thermally programmed isotopic exchange (TPIE) experiments with labeled oxygen ($^{18}O_2$).

Bimetallic catalysts supported on alumina or CeO_2–Al_2O_3 were able to activate oxygen at similar temperature ranges and exchange rates to the monometallic "parent" catalysts. With ceria-supported bimetallic catalysts, the temperature ranges for the oxygen exchange were broadened toward the high-temperature region (500–600 °C), and the maxima (R_e maximum) shifted to higher temperatures.

Table 4. Results of the thermally programmed isotopic exchange experiments for all the prepared catalysts (R_e is the rate of oxygen exchange, and N_e is the number of exchanged atoms).

Catalyst	Starting Temperature Range of Exchange (°C)	Temperature of Maximum Rate (°C)	R_e Maximum (10^{17} at·g^{-1} s^{-1})	N_e Final at 600 °C (10^{21} at·g^{-1})
Pt–Au/Al	380→	555	5.0	1.5
Cu–Au/Al	340→	470	5.1	1.8
Pt–Au/Ce	340→	490	11.6	4.0
Cu–Au/Ce	280→	410/520	5.2/10.1	4.7
Pt–Au/Ce–Al	390→	510	6.8	2.3
Cu–Au/Ce–Al	330→	440	4.2	2.1

The lowest oxygen activation temperatures were observed with the Cu–Au catalysts. The Pt–Au catalysts showed a poorer performance than the bare supports regarding the exchange rate and the number of exchanged atoms. For example, the formation of $^{18}O^{16}O$ with the Pt–Au/Ce catalyst was detected at around 340 °C, a substantially higher temperature than with the ceria support alone. The metal salts used in the preparation of monometallic Pt and bimetallic Au catalysts contained chlorine that may have inhibited the activation of oxygen, as explained in Reference [40].

In general, Pt catalysts could promote the exchange of $^{18}O_2$ on the supports, but the reaction was limited by the adsorption/desorption of O_2 over a large range of temperatures. The performance of Pt catalysts was also sensitive to particle size variations, and the exchange was faster on larger Pt particles. The differences were significant, with a factor of almost 45 on the rate of equilibration when the dispersion of the Pt varied by a factor of 15 [41]. The rather small particle size evidenced by HR-TEM for Pt–Au/Ce–Al and Pt–Au/Al might have been a reason for the relatively poor oxygen activation. Finally, based on the TPIE results, the addition of Au only improved the performance of the Cu/Ce catalyst by broadening the temperature window and increasing the amounts of exchanged oxygen atoms [12]. The XPS results showed that this particular catalyst contained more Cu^{1+} and Cu^0 than other copper catalysts. A lower oxidation state of metal might be advantageous for oxygen activation [42].

2.2. Activity of the Catalysts in the Oxidation of DMDS

Figure 9a–c shows that the complete conversion of DMDS was reached in a temperature range from 500 to 600 °C in most of the catalysts. Table 5 summarizes the results. The Cu–Au/Al catalyst showed the best activity in the oxidation of DMDS, followed by Cu–Au/Ce–Al. Generally, the Cu-containing catalysts showed better activity in terms of DMDS conversion than the Pt-containing catalysts. This might have been partly due to the higher amount of reactive oxygen available in copper catalysts' structures, as evidenced by H_2-TPR and TPIE.

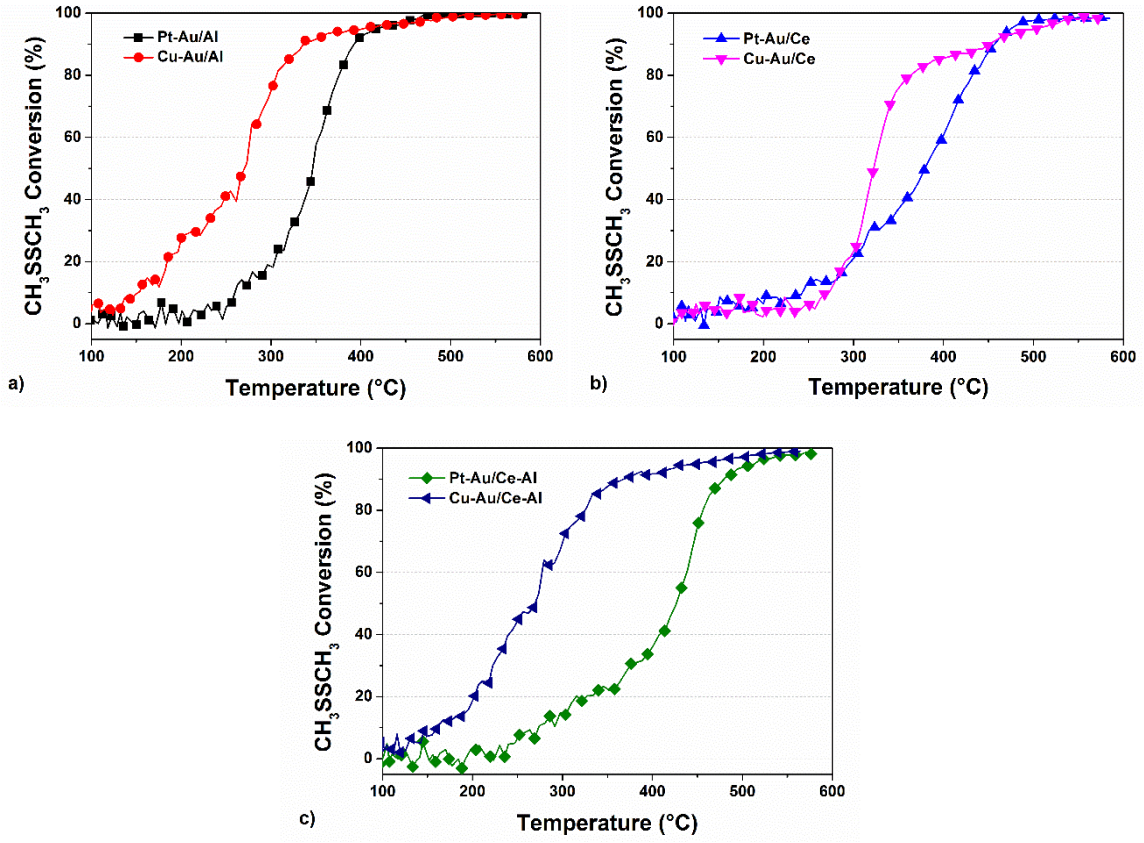

Figure 9. The activity of Pt–Au and Cu–Au catalysts on (**a**) γ-Al_2O_3, (**b**) CeO_2, and (**c**) CeO_2–Al_2O_3 in the oxidation of dimethyl disulfide (DMDS) (DMDS 500 ppm, weight hourly space velocity (WHSV) 720 g g_{cat}^{-1} h^{-1}, 5 °C min^{-1}).

The deposition of Au on Pt in the case of the Pt–Au/Al catalyst had a positive effect on activity. The T_{50} and T_{100} values of the "parent" Pt/Al catalyst decreased by 40 °C and 70 °C, respectively. A negative effect was observed with the Pt/Ce and Pt/Ce–Al catalysts: The light-off temperatures were 55 °C and 45 °C higher, respectively. The deposition of Au on Cu also had a positive impact on the light-off temperature in the case of the Cu–Au/Al catalyst. The T_{50} and T_{100} values of the "parent" Cu/Al catalyst decreased by 5 °C and 30 °C, respectively. However, the deposition of Au had a negative effect on the activity of the Cu/Ce catalyst. When considering the Cu/Ce–Al catalyst, which was the best catalyst in terms of DMDS conversion among the monometallic "parent" catalysts, the deposition of Au lowered the T_{25} value by 60 °C, while T_{50} remained the same (275 °C). Unfortunately, T_{90} shifted from 290 °C to 370 °C. The decrease in activity of the Cu–Au/Ce and Pt–Au/Ce catalysts might have been due to a significant decrease in the specific surface area and pore clogging after the introduction of Au, but also might have been due to the significantly larger metal particles present on the catalyst surface (see Reference [12] for the results of monometallic catalysts).

Table 5. Summary of the T_{50}, T_{90}, and T_{100} temperatures of tested catalysts (°C, rounded to 5 °C).

	Al_2O_3			CeO_2			CeO_2–Al_2O_3		
	T_{50}	T_{90}	T_{100}	T_{50}	T_{90}	T_{100}	T_{50}	T_{90}	T_{100}
Pt [a]	390	415	550	325	435	*	380	460	*
Pt–Au	350	390	480	380	455	*	425	480	*
Cu [a]	280	400	545	300	445	*	275	290	325
Cu–Au	275	340	515	330	450	575	275	370	570

[a] From our previous study [12]. * Not reached below 600 °C.

2.3. Yields of DMDS Oxidation Products

The desired final products in the oxidation of DMDS are SO_2, CO_2, and water. The yields of SO_2 for all the prepared catalysts are displayed in Figure 10a–c. Overall, the highest yields of SO_2 were observed with the Cu-containing catalysts (Figure 10a–c). The addition of Au to the Cu/Al and Cu/Al–Ce "parent" catalysts did not change the SO_2 production profile significantly. In the case of Cu/Ce, the addition of Au caused over a 10%-point decrease in the maximum yields of SO_2. The addition of Au to the corresponding Pt "parent" catalysts had a positive impact on the Al_2O_3-supported catalyst by widening the temperature window for SO_2 formation by about 100 °C. In the case of CeO_2-supported Pt, the addition of Au lowered the amount of SO_2. In the case of Al_2O_3–CeO_2, SO_2 formation shifted to a higher temperature level. When comparing the bimetallic catalysts, Cu–Au/Ce and Pt–Au/Ce maintained a yield of SO_2 at a fairly high value of 80% even at high temperatures, i.e., 550 °C (Figure 11b). The other catalysts showed a decrease in the formation of SO_2 above roughly a temperature of 490 °C, which may indicate the further oxidation of SO_2 to SO_3. Maintaining the good yield of SO_2 in a wide temperature window is important in terms of the durability of a catalyst and industrial treatment equipment.

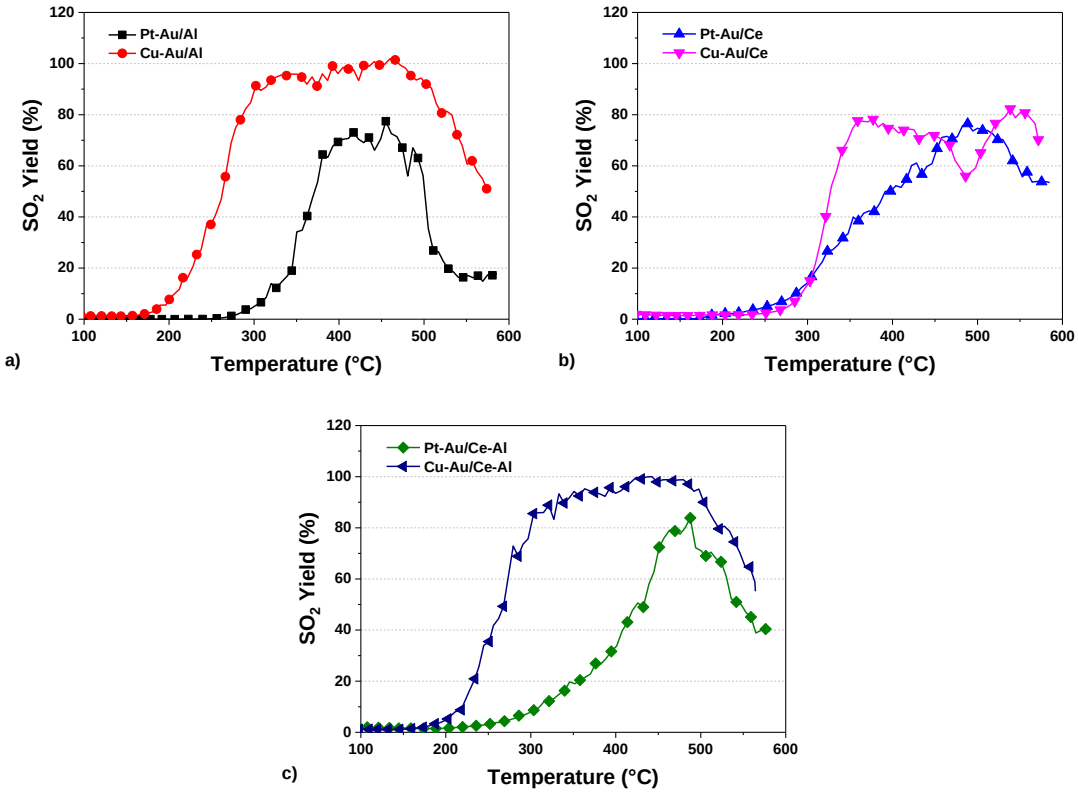

Figure 10. The SO_2 yields over Pt–Au and Cu–Au supported on (**a**) γ-Al_2O_3, (**b**) CeO_2, and (**c**) CeO_2–Al_2O_3 in the oxidation of DMDS (the same experimental conditions as in Figure 9).

The best yields toward CO_2 were obtained over the Pt–Au catalysts starting roughly at the temperature of 400 °C. The Pt–Au/Al, Pt–Au/Ce, and Pt–Au/Ce–Al catalysts achieved yields of ~100% for CO_2 at approximately 515 °C, 570 °C, and 530 °C, respectively. The adsorption/desorption phenomena seen during the experiments resulted in yields over 100% with Pt–Au/Al and Pt–Au/Ce–Al. All the Pt–Au catalysts showed high yields toward CO_2, while the Cu–Au catalysts exhibited partial oxidation to produce mainly CH_2O. It must be noted that in the case of Al_2O_3 and CeO_2–Al_2O_3-supported Cu–Au catalysts, a low formation of CO_2 was seen to start at around 300 °C, and yields of approximately 50–60% were achieved at the end of the experiment.

In addition to the main oxidation products, certain byproducts were observed during the DMDS oxidation experiments. The formation of formaldehyde (CH_2O), carbon monoxide (CO), methanol (CH_3OH), methyl mercaptan (CH_3SH, MM), and dimethyl sulfide (CH_3SCH_3, DMS) between approximately 350 and 500 °C was slightly higher with the Pt–Au/Al catalyst compared to other Pt–Au catalysts. The addition of Au increased the formation of byproducts with the Pt/Al catalyst. In the case of the Pt–Au/Ce catalyst, the addition of Au had a positive effect on selectivity. The distribution of the main products seen in Figure 11a for Pt–Au/Ce was better compared to that of the "parent" Pt/Ce catalyst presented in Figure 11c, which produced higher concentrations of byproducts (CO, CH_2O), excluding a temperature window from 400 to 480 °C. The Pt/Ce catalyst showed a rapid decrease and a subsequent increase in the formation of CH_2O between 400 and 480 °C (Figure 11c), which was connected to a comparable decrease in the formation of CO and an increase in the formation of CO_2. This peculiar behavior seen in the yields of carbon products with the Pt/Ce catalyst between certain temperature ranges disappeared after the addition of Au. With respect to the Pt–Au/Ce–Al catalyst, the addition of Au did not have any significant effect on the yields of the byproducts. The byproducts appeared at a slightly wider temperature range, but the amounts were very similar to the Pt/Ce–Al catalyst.

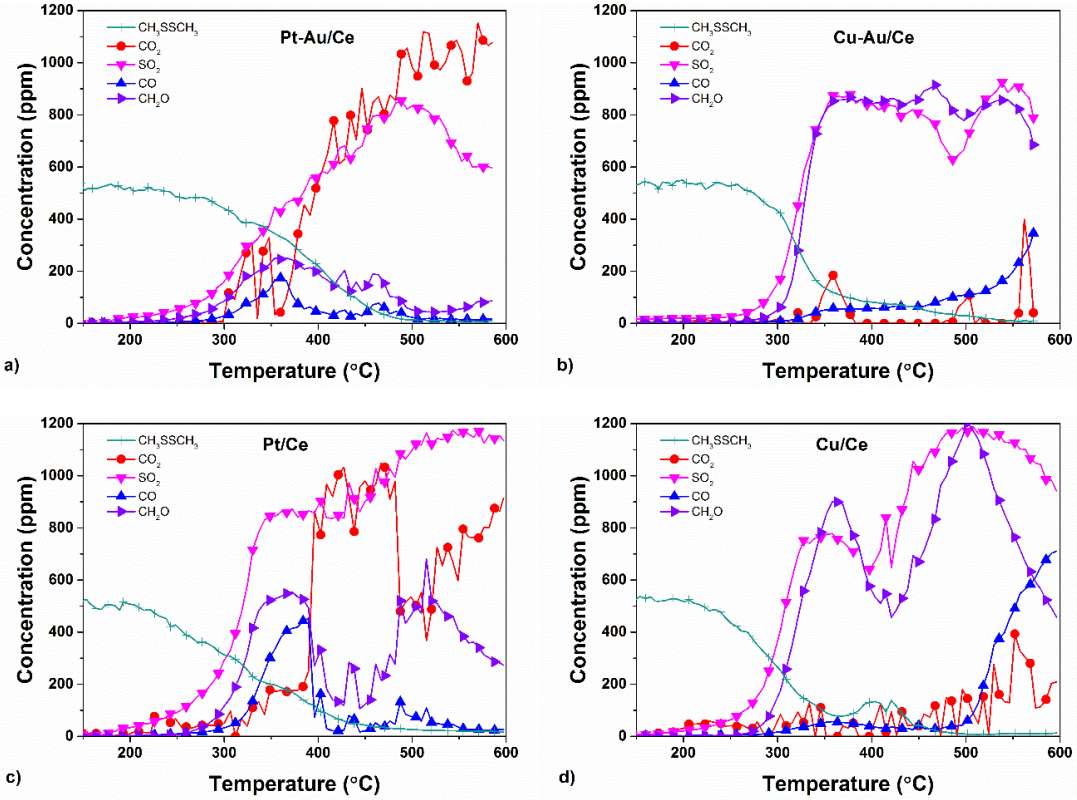

Figure 11. The distribution of the main products, CO_2, SO_2, CO, and CH_2O, with (**a**) Pt–Au on CeO_2, (**b**) Cu–Au on CeO_2, (**c**) Pt on CeO_2 and (**d**) Cu on CeO_2 catalysts in the oxidation of DMDS (CH_3SSCH_3). The concentrations of other byproducts were less than 50 ppm (the same experimental conditions as in Figure 9).

The addition of Au to Cu/Al increased the formation of CO at high temperatures. At the same time, CH_2O formation remained at a similar level. On the contrary, in the case of the Cu–Au/Ce–Al catalyst, lower concentrations of CO were seen at high temperatures than with the "parent" Cu/Ce–Al catalyst reported in Reference [12]. Unfortunately, the decreased formation of CO was not seen to result in an increased formation of CO_2. Furthermore, CH_2O formation was decreased for the Cu–Au/Ce–Al catalyst. Interestingly, the deposition of Au on Cu/Ce had a higher impact on the selectivity of main oxidation products (see Figure 11). The double peaks observed in the formation of SO_2 and CH_2O with

the Cu/Ce catalyst (Figure 11d) disappeared after the addition of Au, similarly to the case of Pt–Au/Ce. Au addition to the Pt/Ce and Cu/Ce catalysts seemed to stabilize the formation of SO_2.

Since the formation of CO and CH_2O were the most significant of the byproducts detected, they will be considered a bit in more detail. The yields of CH_2O and concentrations of CO during the oxidation of DMDS are displayed in Figure 12a–c,d–f. Generally, the lowest amounts of byproducts were formed over the Pt–Au catalysts. The formation of CH_2O over the Cu–Au catalysts was significant and independent of the support used (Figure 12a–c). In general, the highest amounts of CH_2O were formed over the Cu-containing catalysts. The formation of CH_2O was enhanced by both copper and ceria. The Pt–Au catalysts also had a lower formation of CO compared to the Cu–Au catalysts. The lowest formation of CO was observed for Pt–Au/Ce.

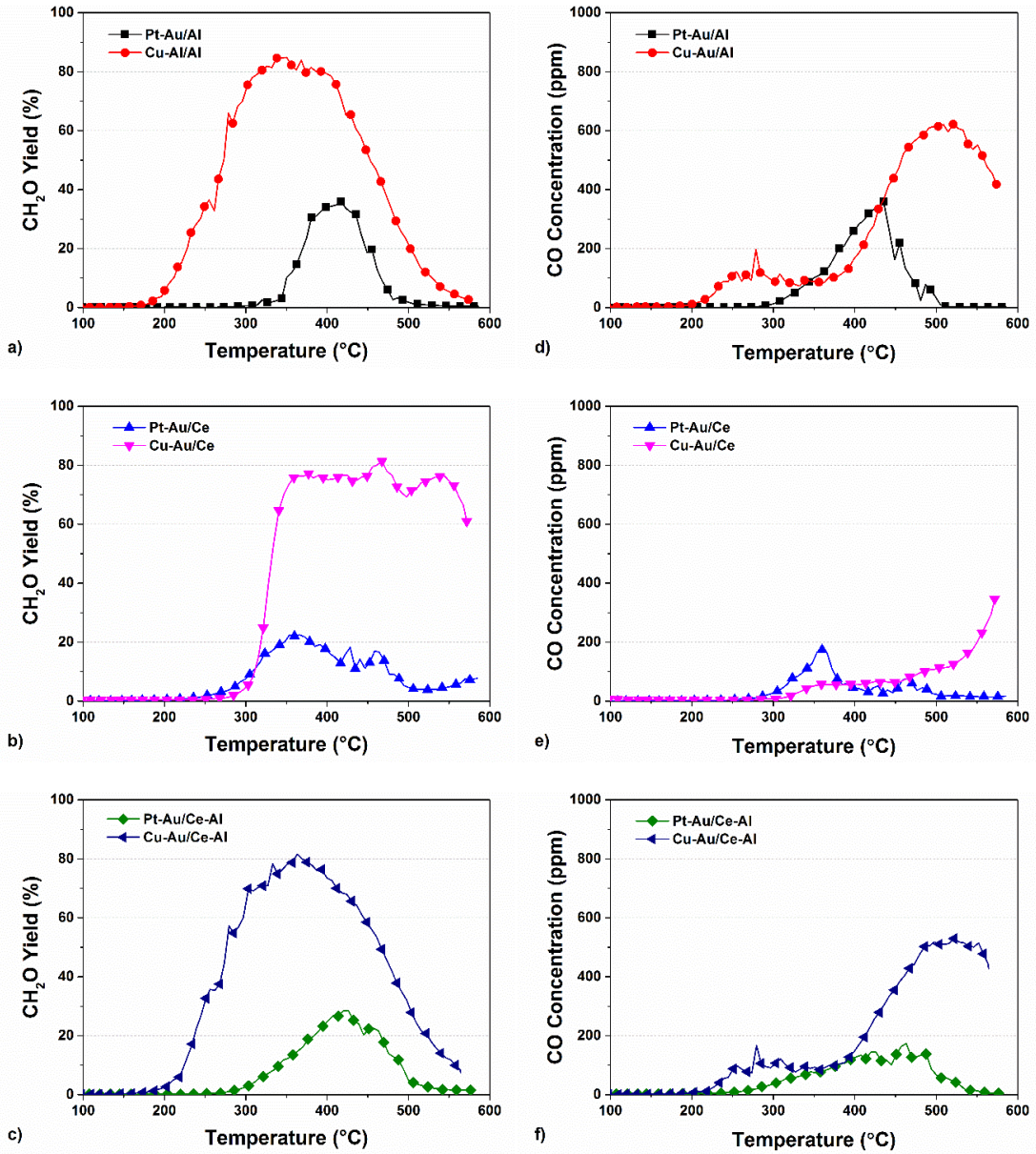

Figure 12. CH_2O yields over the Pt–Au and Cu–Au catalysts on (**a**) γ-Al_2O_3, (**b**) CeO_2, and (**c**) Pt–Au and Cu–Au on CeO_2–Al_2O_3 and CO concentration over the Pt–Au and Cu–Au catalysts on (**d**) γ-Al_2O_3, (**e**) CeO_2, and (**f**) CeO_2–Al_2O_3 in the oxidation of DMDS (the same experimental conditions as in Figure 9).

When considering all the undesired reaction products, the most applicable catalysts in the total oxidation of DMDS were Pt–Au/Ce and Pt–Au/Ce–Al, which formed high yields of SO_2 and CO_2 in a broad temperature range (Figure 11a). The formation of SO_2 was higher above temperatures of 500 °C with Pt–Au/Ce in comparison to Pt–Au/Ce–Al. Of the alumina-supported catalysts, the Pt–Au/Al catalyst produced more CH_2O compared to Pt/Al, but the temperature window for SO_2 formation widened toward higher temperatures. With the Cu–Au/Al catalyst, the Au addition decreased the formation of CH_2O to some extent and had no effect on SO_2 formation. Considering ceria-supported catalysts, the formation of SO_2 and CH_2O remained at a somewhat similar level or decreased depending on the catalyst.

2.4. Stability of the Pt–Au/Ce–Al Catalyst

In our previous study, Au/Ce–Al demonstrated good stability in DMDS oxidation and selectivity toward SO_2. However, the formation of CH_2O was significant, and therefore, the selectivity of the catalyst toward CO_2 needed an improvement [12]. The well-performing Pt–Au/Ce–Al was chosen for the stability test in order to compare the results of the monometallic Au/Ce–Al catalyst. Furthermore, this catalyst contained Pt at lower oxidation states, which should have made the catalyst less sensitive to poisoning. The experimental conditions were chosen based on the 90% DMDS conversion observed during the light-off tests. Prior to the stability test, a single light-off test was done. After 40 h, the feed of DMDS was closed and the reactor was cooled down to room temperature (RT) following a second light-off test to observe changes in the catalyst performance. After the second light-off test, the Pt–Au/Ce–Al catalyst was regenerated in situ by heating the catalyst from RT to 600 °C (5 °C min^{-1}) under an air flow. After the regeneration, a third light-off test was carried out.

During the stability tests, a gradual decrease in the DMDS conversion from 90% to about 70% was observed. The yields of SO_2, CO_2, and CH_2O throughout the test were at around 50–55%, 50–80%, and 5%, respectively. The related light-off curves are shown in Figure 13.

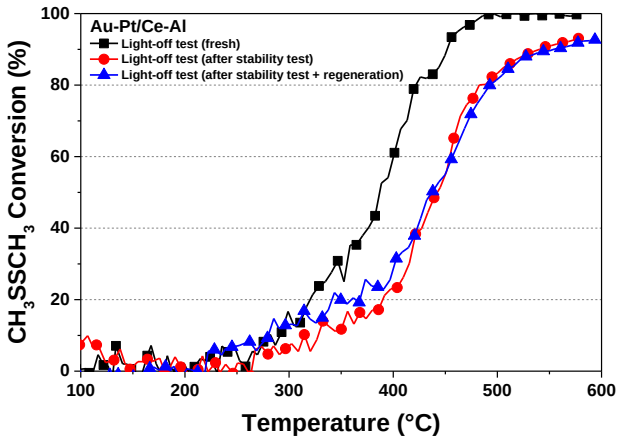

Figure 13. The DMDS conversion over Pt–Au/Ce–Al before (fresh) and after the stability test and after regeneration with air (the experimental conditions are the same as in Figure 9).

As can be seen in Figure 13, the Pt–Au/Ce–Al catalyst lost some activity during the 40-h stability test. The T_{50} temperatures decreased roughly by 50 °C, and the total conversion of DMDS was not achieved. In situ regeneration with air was not able to restore the activity. The deactivation may have resulted for several reasons. For example, sintering of the metal particles causing the loss of active surface areas may have occurred. Sintering may have been facilitated due to residual chlorine left in the bimetallic catalysts after the Au addition. According to the shapes of the curves, mass transfer limitation caused by the deposition of sulfates on the support may have appeared as well [43]. The XRF analysis verified the presence of roughly 3.4 wt % of sulfur in the sample. However, the Raman analysis did not show the presence of sulfates. The catalyst sample used was also analyzed with HR-TEM, and

a recalculation of particle size distribution was done. Figure 14 shows an HR-TEM image of the used Pt–Au/Ce–Al catalyst with PSD information.

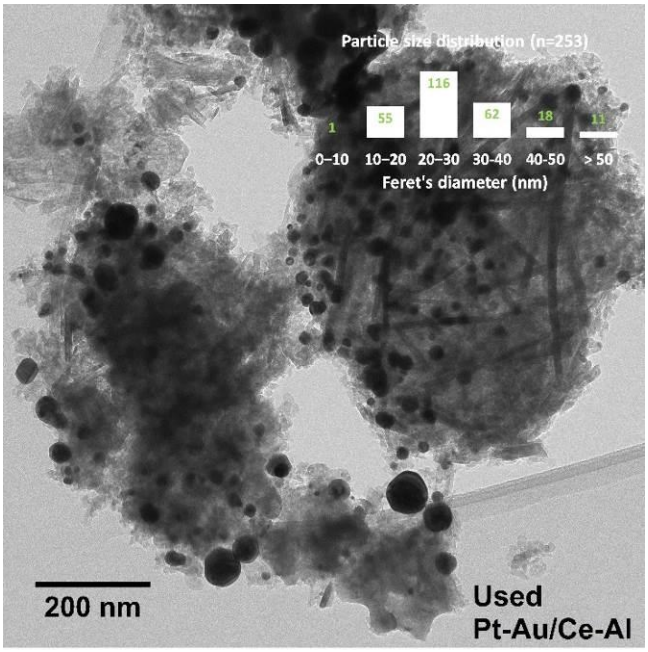

Figure 14. HR-TEM image of the used Pt–Au/Ce–Al catalyst after the stability test and in situ regeneration.

The PSD of the used catalyst evidenced sintering. The particles less than 10 nm were not clearly seen in the used catalyst. The ratio of particles in sizes between 10 and 20 nm and 20 and 30 nm changed drastically from approximately 1:1 to 1:2 in the used catalyst. Furthermore, the amounts of 30–40-nm and 40–50-nm particles increased from ~10% up to ~25% and from ~1% up to ~7%, respectively. Sintering occurred, since the $T_{Tammann}$ of gold is 405 °C, which is less than the T_{90} used during the stability test. In addition, the mobility of Au on the catalyst surface was facilitated by residual chlorine. Furthermore, sulfate may have promoted the mobility of especially Pt particles, leading to agglomeration and simultaneous hindrance of the redispersion during regeneration. Sulfur was seen mainly on the support (based on the EDX data) instead of covering the active phases, maybe due to the electronegative nature of Au restricting chemisorption and bonding with sulfur in contrast to Pt alone, which is sensitive to sulfur deactivation. From these results, we can conclude that the addition of Au via the preparation method used was not able to improve the stability of the Pt/Ce–Al catalyst as expected [12].

3. Discussion

The results summarized in Figure 15 are used to highlight certain activity-, selectivity-, and durability-related aspects and their dependence on temperature for the Pt–Au/Ce–Al catalyst. Similar figures for other catalysts are presented in the Supplementary Materials, Figures S10 and S11. In the Figure 15 DMDS conversion, SO_2, CO_2, CO, and CH_2O yields; the oxygen exchange rate; H_2 uptake; and NH_3 desorption results are presented with respect to temperature in the range of 50 to 600 °C in the case of the Pt–Au/Ce–Al catalyst. The three gray vertical lines in the graph highlight temperature regions that were related to the DMDS conversion and yields of products and byproducts.

Based on the data shown, it seems that the formation temperature of SO_2 correlated with the starting conversion temperature of DMDS, indicating the initiation of partial oxidation, as evidenced by the simultaneous production of CO and CH_2O. At higher temperatures, before the oxygen exchange rate began to increase, the formation of byproducts was at the highest level. At the temperature level

where the oxygen exchange rate was at a maximum, the CO_2 yield began to increase gradually, while the byproduct yields decreased, indicating complete oxidation. Further, at the same temperature range, the DMDS conversion reached its maximum of ~98%. Unfortunately, SO_2 formation started to decrease at the same temperature level. Similar behavior was seen with the Pt–Au/Al and Pt–Au/Ce catalysts shown in Figure S10.

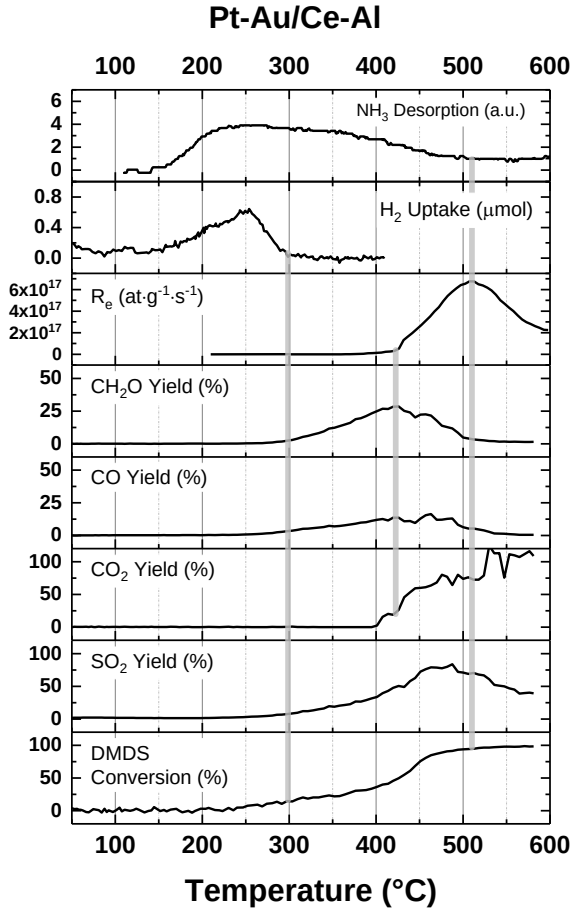

Figure 15. Summary of DMDS conversion, product yields, oxygen exchange rate, H_2 uptake, and NH_3 desorption results for the Pt–Au/Ce–Al catalyst. The temperature scale in the result is common for the different tests, and *y* axis values are related to each experiment.

The same scenario was investigated in the case of the Cu–Au catalysts (Figure S11). First, with the Cu–Au catalysts, the DMDS conversion started with the adsorption of DMDS on the surface, because there were no oxidation products formed yet at a temperature of approximately 150 °C. At a slightly higher temperature, i.e., around 200 °C, the formation of SO_2 started. With the Cu–Au/Ce catalyst, the initiation of the reaction was delayed compared to the alumina-based catalysts, but the reaction was faster when it began at the same temperatures at which the oxygen activation started, thus providing oxygen for the reaction. The Cu–Au catalysts also led to the highest yields of SO_2 at the temperature where the oxygen exchange rate was at a maximum. In general, with the Cu–Au catalysts, the activation of oxygen started at lower temperatures in comparison to the Pt–Au catalysts, which in turn seemed to affect the reaction of DMDS, resulting in lower conversion temperatures. These results suggest that oxygen activation at a lower temperature contributed to a low light-off point of Cu–Au in the DMDS oxidation, which led to partial oxidation products. The relation of lower light-off to higher availability of reactive oxygen was noted earlier.

It is known that catalyst acido–basic properties may have an impact on the performance of a catalyst. The quality of acid sites has especially been shown to affect intermediate or byproduct

distribution and thus the reaction mechanism [44]. We approached this issue by using NH_3 and CO_2-TPD. DMDS, CO_2, SO_2, and CH_2O are acidic molecules, and thus they were expected to adsorb, preferably on basic sites. Thus, the increase or decrease of acid and basic sites after the addition of Au to a parent catalyst may have affected the DMDS adsorption as well as product distribution. In general, the basicity of the catalysts remained at a low level, as expected. Based on CO_2-TPD, the total basicity of Pt/Ce–Al increased after the Au addition from 85 to 105 $\mu molg^{-1}$. In the case of Cu/Ce–Al, basicity increased slightly, from 45 to 90 $\mu molg^{-1}$. The total consumption of CO_2 in the case of the Pt–Au/Al and Cu–Au/Al catalysts was 100 and 130 $\mu molg^{-1}$, respectively. The same values for Pt–Au/Ce and Cu–Au/Ce were 90 and 120 $\mu molg^{-1}$, respectively. The Cu–Au/Al and Cu–Au/Ce catalysts were slightly more basic than the corresponding Pt–Au catalysts. The basicity of Cu–Au/Ce–Al remained at a lower level than the corresponding Pt–Au catalyst. The slightly higher basicity of the Cu–Au/Al and Cu–Au/Ce catalysts could have had a role in the adsorption of DMDS at lower temperatures. The Cu–Au/Ce catalyst had mainly weak basic sites, while Cu–Au/Al and Cu–Au/Ce–Al had both weak and medium strength basic sites.

The acidity of the parent catalysts did not change drastically after the Au addition, despite the low pH used during the preparation of the bimetallic catalysts. According to NH_3-TPD, the Al_2O_3-supported bimetallic catalysts were the most acidic, followed by Ce–Al and CeO_2. Cu–Au/Al had fewer weak and medium acid sites than did Pt–Au/Al. Both the catalysts lost some weak acidity (100–400 °C) after the addition of Au. The amount of weak acidity was also decreased with Pt/Ce–Al after the Au addition. Cu–Au/Ce–Al had a slightly higher amount of weak acid sites than did Pt–Au/Ce–Al. CeO_2-supported bimetallic catalysts represented the lowest acidities. While the acidity of Pt–Au/Ce was low and the thermal conductivity detector (TCD) signal remained practically constant during the analysis, the Cu–Au/Ce catalyst represented two peaks, a smaller one representing weak acid sites and an intense one at around 800°C representing the stronger acid sites. The lower acidity and higher basicity of the Cu–Au/Ce catalyst could be one explanation for the delayed reaction of DMDS over Cu–Au/Ce compared to Al_2O_3 and CeO_2–Al_2O_3-supported Cu–Au.

4. Materials and Methods

4.1. Catalyst Preparation

Six different bimetallic catalysts on three different supports, i.e., Al_2O_3, CeO_2, and CeO_2–Al_2O_3 containing 20 wt % of CeO_2, were prepared using surface redox reactions in an aqueous phase. Nomenclature and target compositions of the catalysts are shown in Table 6. Based on our previous results, the total conversion of DMDS is achieved at around 600 °C [5], and therefore the catalysts were calcined in air for 5 h at 600 °C with a heating rate of 5 °C min^{-1}.

Table 6. Target compositions of the prepared bimetallic catalysts.

Catalyst Abbreviation	Support	Target Amount of Metals (wt %)		
		Au	Pt	Cu
Pt–Au/Al	Al_2O_3	1	1	-
Cu–Au/Al	Al_2O_3	1	-	5
Pt–Au/Ce	CeO_2	1	1	-
Cu–Au/Ce	CeO_2	1	-	5
Pt–Au/Ce–Al	CeO_2–Al_2O_3	1	1	-
Cu–Au/Ce–Al	CeO_2–Al_2O_3	1	-	5

Calcined monometallic Pt and Cu catalysts were used as the "parent" catalysts for the synthesis of bimetallic catalysts. The monometallic catalysts, containing 1 wt % of platinum or 5 wt % of copper on commercial γ-Al_2O_3 (Rhodia), commercial CeO_2 (Rhodia), and synthesized CeO_2–Al_2O_3, were prepared using wet impregnation. Detailed preparation steps are described in Reference [12].

Bimetallic catalysts were obtained using surface redox reactions [45]. In the preparation, a requisite amount of a monometallic parent catalyst was placed inside a glass reactor. The reactor was first flushed with a countercurrent N_2 flow for 15 min at room temperature. Next, the catalyst was reduced in an H_2 flow of 100 cm^3 min^{-1} by increasing the temperature at a rate of 5 °C min^{-1} up to 300 °C in the case of Pt-containing catalysts and up to 400 °C with the Cu-containing catalysts. After the reduction, the reactor was cooled down to room temperature, and ultrapure water was used to wash the catalyst bed. Then, the reactor was degassed by feeding N_2 for 10 min at room temperature. A desired amount of Au salt ($HAuCl_4 \cdot 3H_2O$, Acros) was dissolved in ultrapure water, and the pH of the solution was adjusted to 1 with hydrochloric acid. The Au solution was introduced to the system under an N_2 flow. The solution was kept in the reactor for 1 h under an H_2 flow of 300 cm^3 min^{-1}. The resulting bimetallic catalyst was separated from the aqueous solution with a sieve. The samples were dried under an H_2 flow of 300 cm^3 min^{-1} at 100 °C overnight. Finally, the catalysts were reduced by increasing the temperature from 100 °C up to 300 °C for 1 h. The obtained bimetallic catalysts were calcined in a muffle furnace through heating from room temperature up to 600 °C at a heating rate of 5 °C min^{-1} and dwelling at 600 °C for 5 h under atmospheric conditions.

4.2. Characterization

The elemental compositions of catalysts were determined using ICP-OES equipment, the Perkin Elmer Optima 2000 DV (Waltham, MA, USA), after a microwave-assisted sample digestion in aqua regia. A PANalytical AXIOSmAX 4kW PW2450 wavelength dispersive X-ray fluorescence (XRF) spectrometer (Almelo, the Netherlands) with an Omnian (standardless calibration) application was used to analyze the main elemental composition and amount of sulfur in the catalyst sample after the stability test. The measurement was done using the "loose powder" method in an He atmosphere. The analysis results were given normalized to 100% of the sum of all known analytes in their known oxide or elemental state. The analysis channel for Ce K alpha in the Omnian method overlapped with Au, and thus Ce was analyzed using a Ce L alpha channel.

The specific surface area (S_{BET}) was determined using the BET-BJH method with nitrogen adsorption at −196 °C and was performed with a Micromeritics ASAP 2020 apparatus (Norcross, GA, USA). Prior to the analyses, the catalyst samples were pretreated at 300 °C under a vacuum for at least 2 h to eliminate adsorbed compounds. X-ray diffraction (XRD) was used to recognize the phase composition of the catalysts. The XRD patterns were recorded with a Siemens D5000 diffractometer (Munich, Germany) equipped with a Cu anode (λ_{Cu} = 1.5418 Å) and a nickel filter. The diffractograms were obtained with the following specifications: a 2θ range of 20−85°, step of 0.05°, and step time of 3 s. The Scherrer equation was used to calculate crystallite sizes. X-ray photoelectron spectroscopy (XPS) was used for the determination of the oxidation states of gold, platinum, copper, cerium, and aluminum, but also to evaluate the chemical states of oxygen and composition of the materials. XPS analysis was performed with a Thermo Fisher Scientific ESCALab 250Xi spectrometer (Waltham, MA, USA) with an Al Kα (1486.6 eV) radiation source and a pass energy of 20 eV. The data were analyzed with Thermo Scientific Avantage™ software, and the signals were fitted with the mixed Gaussian–Lorentzian function. Binding energies were referred to the C1s peak line at 284.8 eV, and the Smart function was used to reduce the background. Raman spectra were collected with a Timegate™ 532 Raman Spectrometer (Oulu, Finland) that uses a pulsed 532-nm laser and a single-photon-counting CMOS SPAD matrix detector with a 100-ps time resolution. The system allows for the suppression of fluorescence interference. The data were collected between a Raman shift range of 100 and 1100 cm^{-1} and 700 and 1700 cm^{-1}, with a spectral resolution of 10 cm^{-1}. In the data treatment, second derivatives and wavelets were used for background and noise reduction.

High-resolution transmission electron microscope (HR-TEM) images were obtained using JEOL JEM-2100, JEOL JEM-2100F, and JEOL JEM-2200FS devices (Tokyo, Japan) with an accelerative voltage of 200 kV. The electron microscopes were equipped with an energy-dispersive X-ray spectrometer (EDX).

H_2-TPR experiments were conducted to determine the reducibility of the catalysts. Prior to each H_2-TPR experiment, the catalyst sample (200 mg) was pretreated in situ under an oxygen flow during heating from RT to 600 °C at a rate of 5 °C min^{-1} and was kept there for 10 min to eliminate the residual species. Subsequently, the sample was cooled down to 35 °C under an oxygen flow in two steps: First from 600 to 350 °C, followed by dwelling for 2 h and further cooling down to 35 °C. Then, oxygen was purged from the system under an argon flow over 10 min. Finally, the H_2-TPR experiment was carried out from 35 °C up to 400 °C with a heating rate of 5 °C min^{-1} under 1 vol % of H_2 in argon. Magnesium perchlorate was used to trap the produced water at the outlet of the reactor. Hydrogen consumption was followed using a thermal conductivity detector (TCD). Total acidity measurements were conducted using NH_3-TPD with Micromeritics AutoChem II 2920 (Micromeritics, Norcross, GA, USA) and Quantachrome Chembet Pulsar TPR/TPD devices (Boynton Beach, FL, USA), both equipped with a TCD detector. The samples were pretreated under an He flow at 500 °C for 30 min using 50 mg of a catalyst in an Autochem II device and 200 mg in a Quantachrome device and were cooled down to 100 °C in an He flow. After that, the samples were treated with ammonia for 60 min at 100 °C using 50 mL min^{-1} of 15% NH_3 in He with the Autochem II device and 120 ml min^{-1} of 10% NH_3 in He with the Quantachrome device. The physisorbed NH_3 was removed by feeding He for 30 min at 100 °C. Finally, NH_3 desorption was conducted from 100 °C to 950 °C (ramp rate of 10 °C min^{-1}). The CO_2-TPD experiment was done to determine the total basicity of the catalysts. The amount of sample used in the experiments was 50 mg. Prior to the analysis, the samples were flushed in an He flow at 450 °C for 30 min. Then, 5% CO_2 in He (50 ml min^{-1}) was adsorbed on the sample over 60 min at 50 °C. After flushing with He for 30 min, the TPD was done from 50 to 600 °C at a heating rate of 10 °C min^{-1}. The experiment was done with an Autochem II apparatus equipped with a TCD detector. Temperature-programmed isotopic exchange (TPIE) experiments with labeled oxygen ($^{18}O_2$) were done in a closed-loop tubular quartz reactor. Details of the experimental procedure were described in our previous work [12]. As a summary, the mass of the sample in each experiment was 20 mg. The exchange was conducted using pure $^{18}O_2$ from 200 to 600 °C at a heating rate of 2 °C min^{-1} after an oxidizing pretreatment. The concentrations of different isotopomers were measured continuously using a mass spectrometer (Pfeiffer Vacuum, Asslar, Germany).

4.3. Catalytic Tests

The activities of the catalysts were evaluated with light-off tests. The experimental data were obtained using a tubular quartz reactor working at atmospheric pressure with a weight hourly space velocity (WHSV) of 720 g g_{cat}^{-1} h^{-1}. The reactor setup and experimental procedures are described in Reference [12]. A catalyst sample (100 mg) was fixed in the reactor between two quartz wool plugs on the top of a quartz sand bed (400 mg). The initial concentration of DMDS used in the experiments was set to 500 ppm in air to give a total gas flow of 1 dm^3 min^{-1}. The furnace was heated from RT up to 600 °C at a heating rate of 5 °C min^{-1}. Catalytic tests were done for all six bimetallic catalysts. Each test was repeated to validate the results. Prior to the light-off tests, the catalysts were pretreated in air up to 600 °C at a heating rate of 10 °C min^{-1}. During the 40-h stability test, the oven temperature was set to correspond to the T_{90} temperature achieved during the activity experiment. Before and after the stability test, light-off tests were performed. The gas analysis was done with a multicomponent FTIR gas analyzer, the Gasmet CR-2000 (Gasmet Technologies, Helsinki, Finland), which was equipped with a liquid nitrogen cooled mercury cadmium telluride (MCT) detector.

The conversion of DMDS and yields of CO_2, SO_2, and formaldehyde (CH_2O) were calculated as follows:

$$X_{DMDS}\ [\%] = 100 \times \frac{\dot{n}_{DMDS}^{in} - \dot{n}_{DMDS}^{out}}{\dot{n}_{DMDS}^{in}}, \quad (1)$$

$$Y_x\ [\%] = 100 \times \frac{\dot{n}_{x}^{out}}{2 \times \dot{n}_{DMDS}^{in}}, \quad (2)$$

where X is the conversion, Y is the yield, $\dot{n}$ is the molar flow rate [mol min^{-1}], and x represents the compound (SO_2, CH_2O).

5. Conclusions

The aim of the work was to study if the addition of Au to Pt and Cu supported on Al_2O_3, CeO_2, and Al_2O_3–CeO_2 would improve the performance of the catalysts. The catalytic performance was evaluated in terms of activity, selectivity, and stability. The addition of Au to monometallic "parent" catalysts was done by surface redox reactions aimed at the deposition of Au onto Pt or Cu. According to TEM and XPS analyses, the contact of Au with Pt and Cu was observed on all the catalysts. The addition of Au was done in acidic conditions with a Cl-containing precursor salt. The presence of residual Cl increased the sintering of metal particles during calcination, especially in the case of CeO_2 support, leading to rather large particles visible with XRD despite a low loading of Au. The acidic conditions used during the preparation did not change total acidity or basicity of the catalysts drastically. After the addition of Au, the specific surface area of CeO_2-supported parent catalysts decreased considerably. Similar changes were not observed with the Al_2O_3 and CeO_2–Al_2O_3-supported catalysts.

The addition of Au improved the light-off performance of Al_2O_3-supported Cu and Pt catalysts in DMDS oxidation. A negative effect was observed in the cases of CeO_2 and CeO_2–Al_2O_3-supported catalysts. In general, Cu-containing catalysts were more active based on DMDS conversion. However, DMDS oxidation over bimetallic Cu–Au catalysts led to the formation of undesired reaction products. This result was most likely due to several reasons: (1) Copper-containing catalysts have a higher amount of reactive oxygen in their structure; (2) the reactions on copper species occurred via a redox mechanism; (3) gas-phase oxygen dissociation starts at a lower temperature on copper-containing catalysts; and (4) adsorption–desorption behavior was affected by the presence of acid and basic sites on the catalyst surface.

The selectivity toward total oxidation products was better in the case of Pt-containing catalysts. The addition of Au improved the selectivity of ceria-containing catalysts by decreasing the formation of byproducts. This may have had a connection to a lower amount of reactive oxygen after the Au addition (based on the H_2-TPR results).

The temperature window for SO_2 production was widened after the addition of Au to Pt/Al, while in the case of Cu/Al, the same effect was not observed. In the case of CeO_2-supported catalysts, the major outcome was seen with the Pt/Ce catalyst in the temperature window in which SO_2 production widened. The result was similar to the corresponding CeO_2–Al_2O_3-supported catalyst.

Finally, the Pt–Au/Ce–Al catalyst was chosen for a stability test. After 40 h of DMDS oxidation, sintering of the Pt–Au particles and deposition of sulfur on the support were observed. The addition of Au with the preparation method used did not improve the stability of the Pt/Ce–Al catalyst.

Supplementary Materials: The following are available online at http://www.mdpi.com/2073-4344/9/7/603/s1, Figure S1: N_2 adsorption isotherms of the prepared bimetallic catalysts; Figure S2: Pore size distributions of the prepared bimetallic catalysts; Figure S3: HR-TEM images of the Pt–Au/Al catalyst, showing examples of particles with their corresponding EDX data; Figure S4: HR-TEM images of the Cu–Au/Al catalyst, showing examples of particles with their corresponding EDX data; Figure S5: HR-TEM images of the Pt–Au/Ce catalyst, showing examples of particles; Figure S6: HR-TEM image of the Cu–Au/Ce catalyst with corresponding EDX data; Figure S7: HR-TEM images of the Pt–Au/Ce–Al catalyst, showing examples of particles; Figure S8: HR-TEM images of the Pt–Au/Ce–Al catalyst, showing examples of particles with their corresponding EDX data; Figure S9: HAADF-STEM image of the Pt–Au/Ce catalyst; Figure S10: DMDS conversion, product yields (SO_2, CO_2, CO, and CH_2O), oxygen exchange rate, H_2 uptake, and NH_3 desorption results for the Pt–Au/Al and Pt–Au/Ce catalysts (Figure 15 shows corresponding graph for the Pt–Au/Ce–Al catalyst); Figure S11: DMDS conversion, product yields (SO_2, CO_2, CO, and CH_2O), oxygen exchange rate, H_2 uptake, and NH_3 desorption results for the Cu–Au/Al, Cu–Au/Ce, and Cu–Au/Ce–Al catalysts.

Author Contributions: T.K.N. did most parts of the investigation (surveying the literature, preparing the catalysts, most of the characterization, and all catalytic tests) and was responsible for writing (original draft preparation) and taking part in the conceptualization. S.O. led the conceptualization, did some of the characterization (CO_2-TPD, Raman), and took part in the interpretation of the results, the organization of the manuscript, and the writing (review and editing). T.L. did XPS and CO_2-TPD characterization, data interpretation, and helped in the writing

(original draft preparation) of the XPS part. S.S. did XRD analysis and helped with interpretation. S.P. and R.L.K. helped in the writing (review and editing) of the manuscript. R.L.K., S.O., and S.P. are supervisors of T.K.N.'s doctoral thesis and contributed to the organization, planning, project administration, and funding acquisition for this work.

Funding: This research was funded by the Council of Oulu region from the European Regional Development Fund (A32164), the City of Oulu, and the Maj and Tor Nessling Foundation. The Finnish Foundation for Technology Promotion, Walter Ahlström Foundation, KAUTE Foundation, Tauno Tönning Foundation, and University of Oulu Graduate School are acknowledged for their financial support for the research reported in this paper. The work leading to these results also gained funding from the European Union Seventh Framework Programme [FP7/2007-2013] under the grant agreement n° [PIRSES-GA-2012-317714]. The financial support of the Jenny and Antti Wihuri Foundation is acknowledged.

Acknowledgments: Florence Epron and Nicolas Bion are appreciated for their invaluable help and guidance throughout this work and for accessing the characterization infrastructure at the University of Poitiers. Shudong Wang and Sheng Wang are highly appreciated for the use of HR-TEM and NH_3-TPD at the Dalian Institute of Chemical Physics. Nelly Herault, Henri-Joël Sedjame, and Markus Riihimäki are acknowledged for their assistance in the experimental work.

Conflicts of Interest: The authors declare no conflicts of interest.

References

1. Seinfield, J.; Pandis, S. *Atmospheric Chemistry and Physics: From Air Pollution to Climate Change*, 1st ed.; Wiley: New York, NY, USA, 1998.
2. Ojala, S.; Pitkäaho, S.; Laitinen, T.; Niskala, K.N.; Brahmi, R.; Gaálová, J.; Matejova, L.; Kucherov, A.; Päivärinta, S.; Hirschmann, C.; et al. Catalysis in VOC abatement. *Top. Catal.* **2011**, *54*, 1224–1256. [CrossRef]
3. Yoon, S.H.; Chai, X.S.; Zhu, J.Y.; Li, J.; Malcolm, E.W. In-digester reduction of organic sulfur compounds in kraft pulping. *Adv. Environ. Res.* **2001**, *5*, 91–98. [CrossRef]
4. Ojala, S.; Lassi, U.; Ylönen, R.; Keiski, R.L.; Laakso, I.; Maunula, T.; Silvonen, R. Abatement of malodorous pulp mill emissions by catalytic oxidation – pilot experiments in Stora Enso Pulp Mill, Oulu, Finland. *Tappi J.* **2004**, *4*, 9–14.
5. Ojala, S. Catalytic Oxidation of Volatile Organic Compounds and Malodorous Organic Compounds. Ph.D. Thesis, University of Oulu, Oulu, Finland, 2005.
6. Kucherov, A.V.; Sinev, I.M.M.; Ojala, S.; Keiski, R.; Kustov, L.M.M. Adsorptive-Catalytic Removal of CH_3OH, CH_3SH and CH_3SSCH_3 from Air over the Bifunctional System Noble Metals/HZSM-5. In Proceedings of the in from Zeolites to Porous MOF Materials—The 40th Anniversary of International Zeolite Conference, Beijing, China, 12–17 August 2007; Xu, R., Gao, Z., Chen, J., Yan, W., Eds.; Elsevier: Amsterdam, The Nederland, 2007; Volume 170, pp. 1129–1136. [CrossRef]
7. Kucherov, A.V.; Tkachenko, O.P.; Kirichenko, O.A.; Kapustin, G.I.; Mishin, I.V.; Klementiev, K.V.; Ojala, S.; Kustov, L.M.; Keiski, R.L. Nanogold-Containing Catalysts for Low-Temperature Removal of S-VOC from Air. *Top. Catal.* **2009**, *52*, 351–358. [CrossRef]
8. Darif, B.; Ojala, S.; Roy, P.L.; Bensitel, M.; Brahmi, R.; Keiski, R.L. Study on the catalytic oxidation of DMDS over Pt-Cu catalysts supported on Al_2O_3, $AlSi_{20}$ and SiO_2. *Appl. Catal. B Environ.* **2016**, *181*, 24–33. [CrossRef]
9. Darif, B. Synthesis and Characterization of Catalysts used for the Ctalytic Oxidation of Sulfur-Containing Volatile Organic Compounds: Focus on Sulfur-Induced Deactivation. Ph.D. Thesis, University of Oulu, Oulu, Finland, 2016.
10. Darif, B.; Ojala, S.; Kärkkäinen, M.; Pronier, S.; Maunula, T.; Brahmi, R.; Keiski, R.L. Study on sulfur deactivation of catalysts for DMDS oxidation. *Appl. Catal. B Environ.* **2017**, *206*, 653–665. [CrossRef]
11. Corro, G.; Fierro, J.L.G.; Odilon, V.C. An XPS evidence of Pt^{4+} present on sulfated Pt/Al_2O_3 and its effect on propane combustion. *Catal. Commun.* **2003**, *4*, 371–376. [CrossRef]
12. Nevanperä, T.K.; Ojala, S.; Bion, N.; Epron, F.; Keiski, R.L. Catalytic oxidation of dimethyl disulfide (CH_3SSCH_3) over monometallic Au, Pt and Cu catalysts supported on γ-Al_2O_3, CeO_2 and CeO_2-Al_2O_3. *Appl. Catal. B Environ.* **2016**, *182*, 611–625. [CrossRef]
13. Lowell, S.; Shields, J.E.; Thomas, M.A.; Thommes, M. Adsorption Isotherms. In *Characterization of Porous Solids and Powders: Surface Area, Pore Size and Density*; Lowell, S., Shields, J.E., Thomas, M.A., Thommes, M., Eds.; Springer: Dordrecht, The Netherlands, 2004; pp. 11–14.

14. Dow, W.P.; Wang, Y.P.; Huang, T. Yttria-Stabilized Zirconia Supported Copper Oxide Catalyst: I. Effect of Oxygen Vacancy of Support on Copper Oxide Reduction. *J. Catal.* **1996**, *182*, 171–182. [CrossRef]
15. Moulijn, J.A.; Diepen, A.E.; Kapteijn, F. Catalyst deactivation: Is it predictable? What to do? *Appl. Catal. A Gen.* **2001**, *212*, 3–16. [CrossRef]
16. Scirè, S.; Minicò, S.; Crisafulli, C.; Satriano, C.; Pistone, A. Catalytic combustion of volatile organic compounds on gold/cerium oxide catalysts. *Appl. Catal. B Environ.* **2003**, *40*, 43–49. [CrossRef]
17. Jones, A.; McNicol, B. *Temperature-Programmed Reduction for Solid Materials Characterization*, 1st ed.; Marcel Dekker: New York, NY, USA, 1986.
18. Bond, G.C.; Thompson, D.T. Catalysis by Gold. *Catal. Rev.* **1999**, *41*, 319–388. [CrossRef]
19. Haruta, M. Catalysis of Gold Nanoparticles Deposited on Metal Oxides. *CATTECH* **2002**, *6*, 102–115. [CrossRef]
20. Nikolaev, S.A.; Golubina, E.V.; Krotova, I.N.; Shilina, M.I.; Chistyakov, A.V.; Kriventsov, V.V. The effect of metal deposition order on the synergistic activity of Au-Cu and Au-Ce metal oxide catalysts for CO oxidation. *Appl. Catal. B Environ.* **2015**, *168–169*, 303–312. [CrossRef]
21. Liu, Y.; Liu, B.; Liu, Y.; Wang, Q.; Hu, W.; Jing, P.; Liu, L.; Yu, S.; Zhang, J. Improvement of catalytic performance of preferential oxidation of CO in H_2-rich gases on three-dimensionally ordered macro- and meso-porous Pt-Au/CeO_2 catalysts. *Appl. Catal. B Environ.* **2013**, *142–143*, 615–625. [CrossRef]
22. Bai, Y.C.; Zhang, W.D.; Chen, C.H.; Zhang, J.Q. Carbon nanotubes-supported PtAu-alloy nanoparticles for electro-oxidation of formic acid with remarkable activity. *J. Alloys Compd.* **2011**, *509*, 1029–1034. [CrossRef]
23. Musialska, K.; Finocchio, E.; Sobczak, I.; Busca, G.; Wojcieszak, R.; Gaigneaux, E.; Ziolek, M. Characterization of alumina- and niobia-supported gold catalysts used for oxidation of glycerol. *Appl. Catal. A Gen.* **2010**, *384*, 70–77. [CrossRef]
24. Leppelt, R.; Schumacher, B.; Plzak, V.; Kinne, M.; Behm, R.J. Kinetics and mechanism of the low-temperature water-gas shift reaction on Au/CeO_2 catalysts in an idealized reaction atmosphere. *J. Catal.* **2006**, *244*, 137–152. [CrossRef]
25. El-Moemen, A.; Abdel-Mageed, A.M.; Bansmann, J.; Parlinska-Wojtan, M.; Behm, R.J.; Kucerova, G. Deactivation of Au/CeO_2 catalysts during CO oxidation: Influence of pretreatment and reaction conditions. *J. Catal.* **2016**, *341*, 160–179. [CrossRef]
26. Ye, W.; Kou, H.; Liu, Q.; Yan, J.; Zhou, F.; Wang, C. Electrochemical deposition of Au-Pt alloy particles with cauliflower-like microstructures for electrocatalytic methanol oxidation. *Int. J. Hydrog. Energy* **2012**, *37*, 4088–4097. [CrossRef]
27. Karpenko, A.; Leppelt, R.; Plzak, V.; Behm, R.J. The role of cationic Au^{3+} and nonionic Au^0 species in the low-temperature water-gas shift reaction on Au/CeO_2 catalysts. *J. Catal.* **2007**, *252*, 231–242. [CrossRef]
28. Wertheim, G.K.; Dicenzo, S.B.; Youngquist, S.E. Unit charge on supported gold clusters in photoemission final state. *Phys. Rev. Lett.* **1983**, *51*, 2310–2313. [CrossRef]
29. Peng, R.; Sun, X.; Li, S.; Chen, L.; Fu, M.; Wu, J.; Ye, D. Shape effect of Pt/CeO_2 catalysts on the catalytic oxidation of toluene. *Chem. Eng. J.* **2016**, *306*, 1234–1246. [CrossRef]
30. Mei, Z.; Li, Y.; Fan, M.; Zhao, L.; Zhao, J. Effect of the interactions between Pt species and ceria on Pt/ceria catalysts for water gas shift: The XPS studies. *Chem. Eng. J.* **2015**, *259*, 293–302. [CrossRef]
31. Serrano-Ruiz, J.C.; Huber, G.W.; Sánchez-Castillo, M.A.; Dumesic, J.A.; Rodríguez-Reinoso, F.; Sepúlveda-Escribano, A. Effect of Sn addition to Pt/CeO_2-Al_2O_3 and Pt/Al_2O_3 catalysts: An XPS, ^{119}Sn Mössbauer and microcalorimetry study. *J. Catal.* **2006**, *241*, 378–388. [CrossRef]
32. Moulder, J.F.; Stickle, W.F.; Sobol, P.E.; Bomben, K.D. *Handbook of X-Ray Photoelectron Spectroscopy*; Perkin-Elmer Corporation: Eden Prairie, MN, USA, 1992.
33. Biesinger, M.C.; Lau, L.W.M.; Gerson, A.R.; Smart, R.S.C. Resolving surface chemical states in XPS analysis of first row transition metals, oxides and hydroxides: Sc, Ti, V, Cu and Zn. *Appl. Surf. Sci.* **2010**, *257*, 887–898. [CrossRef]
34. Smit, E.; Groot, F.M.F.; Blume, R.; Hävecker, M.; Knop-Gericke, A.; Weckhuysen, B.M. The role of Cu on the reduction behavior and surface properties of Fe-based Fischer-Tropsch catalysts. *Phys. Chem. Chem. Phys.* **2010**, *12*, 667–680. [CrossRef]

35. Potemkin, D.I.; Semitut, E.Y.; Shubin, Y.V.; Plyusnin, P.E.; Snytnikov, P.V.; Makotchenko, E.V.; Osadchii, D.Y.; Svintsitskiy, D.A.; Venyaminov, S.A.; Korenev, S.V.; et al. Alumina and ceria supported Au-Cu nanoparticles prepared via the decomposition of $[Au(en)_2]_2[Cu(C_2O_4)_2]_3{\cdot}8H_2O$ single-source precursor: Synthesis, characterization and catalytic performance in CO PROX. *Catal. Today* **2014**, *235*, 103–111. [CrossRef]
36. Gaudin, P.; Fioux, P.; Dorge, S.; Nouali, H.; Vierling, M.; Fiani, E.; Moliére, M.; Brilhac, J.F.; Patarin, J. Formation and role of Cu^+ species on highly dispersed CuO/SBA-15 mesoporous materials for SO_x removal: An XPS study. *Fuel Process. Technol.* **2016**, *153*, 129–136. [CrossRef]
37. Väliheikki, A.; Kolli, T.; Huuhtanen, M.; Maunula, T.; Keiski, R.L. Activity Enhancement of W–CeZr Oxide Catalysts by SO_2 Treatment in NH_3-SCR. *Top. Catal.* **2015**, *58*, 1002–1011. [CrossRef]
38. Guo, R.T.; Chen, Q.L.; Ding, H.L.; Wang, Q.S.; Pan, W.G.; Yang, N.Z.; Lu, C.Z. Preparation and characterization of CeOx@MnOx core-shell structure catalyst for catalytic oxidation of NO. *Catal. Commun.* **2015**, *69*, 165–169. [CrossRef]
39. Liao, X.; Chu, W.; Dai, X.; Pitchon, V. Bimetallic Au–Cu supported on ceria for PROX reaction: Effects of Cu/Au atomic ratios and thermal pretreatments. *Appl. Catal. B Environ.* **2013**, *142–143*, 25–37. [CrossRef]
40. Duprez, D. Oxygen and Hydrogen Surface Mobility in Supported Metal Catalysts. Study by $^{18}O/^{16}O$ and $^{2}H/^{1}H$ Exchange. In *Isotopes in Heterogeneous Catalysis*; Hargreaves, J.S.J., Jackson, S.D., Webb, G., Eds.; Imperial College Press: London, UK, 2006; pp. 157–158.
41. Descorme, C.; Duprez, D. Oxygen surface mobility and isotopic exchange on oxides: Role of the nature and the structure of metal particles. *Appl. Catal. A Gen.* **2000**, *202*, 231–241. [CrossRef]
42. Ojala, S.; Bion, N.; Baylet, A.; Tarighi, M.; Keiski, R.L.; Duprez, D. Correlations between oxygen activation and methane oxidation over Pd/γ-Al2O3 catalysts prepared by nitrite method. *Appl. Catal. B Environ.* **2011**, *108–109*, 22–31. [CrossRef]
43. Heck, R.M.; Farrauto, R.J. *Catalytic Air Pollution Control: Commercial Technology*; Van Nostrand Reinhold: New York, NY, USA, 1995.
44. Assal, Z.; Ojala, S.; Pitkäaho, S.; Pirault-Roy, L.; Darif, B.; Comparot, J.D.; Bensitel, M.; Keiski, R.L.; Brahmi, R. Comparative study on the support properties in the total oxidation of dichloromethane over Pt catalysts. *Chem. Eng. J.* **2017**, *313*, 1010–1022. [CrossRef]
45. Epron, F.; Especel, C.; Lafaye, G.; Marécot, P. Multimetallic Nanoparticles Prepared by Redox Processes Applied in Catalysis. In *Nanoparticles and Catalysis*; Astruc, D., Ed.; Wiley-VCH Verlag GmbH & Co. KGaA: Weinheim, Germany, 2008; pp. 279–302.